Dynamical Dark Matter from strongly-coupled dark sectors

Keith R. Dienes,[1,2,*] Fei Huang,[1,†] Shufang Su,[1,‡] and Brooks Thomas[3,§]

[1]*Department of Physics, University of Arizona, Tucson, Arizona 85721 USA*
[2]*Department of Physics, University of Maryland, College Park, Maryland 20742 USA*
[3]*Department of Physics, Lafayette College, Easton, Pennsylvania 18042 USA*
(Received 22 October 2016; published 22 February 2017)

Dynamical Dark Matter (DDM) is an alternative framework for dark-matter physics in which the dark sector comprises a vast ensemble of particle species whose Standard-Model decay widths are balanced against their cosmological abundances. Previous studies of this framework have focused on a particular class of DDM ensembles—motivated primarily by Kaluza-Klein towers in theories with extra dimensions—in which the density of dark states scales roughly as a polynomial of the mass. In this paper, by contrast, we study the properties of a different class of DDM ensembles in which the density of dark states grows *exponentially* with mass. Ensembles with this Hagedorn-like property arise naturally as the "hadronic" resonances associated with the confining phase of a strongly-coupled dark sector; they also arise naturally as the gauge-neutral bulk states of Type I string theories. We study the dynamical properties of such ensembles, and demonstrate that an appropriate DDM-like balancing between decay widths and abundances can emerge naturally—even with an exponentially rising density of states. We also study the effective equations of state for such ensembles, and investigate some of the model-independent observational constraints on such ensembles that follow directly from these equations of state. In general, we find that such constraints tend to introduce correlations between various properties of these DDM ensembles such as their associated mass scales, lifetimes, and abundance distributions. For example, we find that these constraints allow DDM ensembles with energy scales ranging from the GeV scale all the way to the Planck scale, but that the total present-day cosmological abundance of the dark sector must be spread across an increasing number of different states in the ensemble as these energy scales are dialed from the Planck scale down to the GeV scale. Numerous other correlations and constraints are also discussed.

I. INTRODUCTION

Dynamical Dark Matter (DDM) [1,2] is an alternative framework for dark-matter physics in which dark-matter stability is not required. Instead, the dark sector within the DDM framework comprises a vast ensemble of individual constituent particles exhibiting a variety of different masses, lifetimes, and cosmological abundances. The phenomenological viability of such a dark sector is then ensured through a nontrivial *balancing* between cosmological abundances and Standard-Model (SM) decay widths across the ensemble. Indeed, under this balancing, those ensemble constituents with shorter lifetimes must have smaller cosmological abundances, while states with longer lifetimes may have larger cosmological abundances. As a result, the dark sector in such a scenario is *dynamic*: states in the dark sector are continually decaying into visible-sector states throughout the evolution of the universe—not just in previous epochs but even at the present time and into the future. Quantities such as the total energy density $\Omega_{\rm CDM}$ and

the effective equation-of-state parameter $w_{\rm eff}$ are thus time-dependent quantities, and it is only an accident that these quantities happen to take particular values at the present time. Many methods have been developed for testing this framework, spanning from collider signatures [3,4] to signatures in direct-detection [5] and indirect-detection [6–8] experiments.

Of course, many of the constraints on such DDM ensembles depend on model-specific details associated with the ensemble in question, such as the specific particle nature of the individual dark constituent fields and the precise form of their decays into SM states. By contrast, other phenomenological properties of (and constraints on) these DDM ensembles depend simply on the manner in which the lifetimes and abundances of ensemble constituents scale with respect to each other, and thus have a greater degree of model independence. For example, the effective equations of state for these ensembles are governed in large part solely by these scaling relations. As a result, all phenomenological/observational constraints on the equations of state of the dark sector are essentially constraints on the types of balancing relations that DDM ensembles may exhibit. These are thus model-independent constraints which can be placed on such ensembles simply as a result of their inherent scaling relations.

[*]dienes@email.arizona.edu
[†]huangfei@email.arizona.edu
[‡]shufang@email.arizona.edu
[§]thomasbd@lafayette.edu

043526-1

One general class of DDM ensembles consisting of large numbers of dark particle species exhibiting suitable scaling relations between lifetimes and cosmological abundances are those whose constituents are the Kaluza-Klein (KK) modes of a gauge-neutral bulk field in a theory with extra spacetime dimensions in which cosmological abundances are established through misalignment production [1]. Indeed, explicit realizations of DDM ensembles of this type have been constructed [2,9]. Although many aspects of these ensembles depend on the details of the particular fields under study, certain general properties are common across all such ensembles in this class. One of these is that the cosmological abundance of each component scales as a power of the lifetime of that component. Likewise, the density of states within such ensembles is either insensitive to mass or scales roughly as a polynomial function of mass across the ensemble. For these reasons, most phenomenological studies of the DDM framework have focused on ensembles exhibiting polynomial scaling relationships.

Polynomial scaling relations also emerge in other (purely four-dimensional) contexts as well. For example, under certain circumstances, thermal freeze-out mechanisms for abundance generation can also lead to appropriate polynomial inverse scaling relations between lifetimes and abundances [10]. In fact, such inverse scaling relations can even emerge *statistically* in contexts in which the dynamics underlying the dark sector is essentially random [11].

There are, however, other well-motivated theoretical constructions which do not give rise to dark sectors with polynomial scaling relations. One example is a dark sector consisting of a set of fermions (dark "quarks") charged under a non-Abelian gauge group G which becomes confining below some critical temperature T_c. At temperatures $T \lesssim T_c$, when the theory is in the confining phase, the physical degrees of freedom are composite states (dark "hadrons"). Another well-motivated type of DDM ensemble consists of the bulk (i.e., closed-string) states in Type I string theories. Such bulk states are typically neutral with respect to all brane gauge symmetries, and interact with those brane states only gravitationally. As such, from the perspective of brane-localized observers, these bulk states too are dark matter.

At first glance, these two latter types of ensembles may seem to have little in common with each other. Indeed, many aspects of the detailed phenomenologies associated with these ensembles will be completely different. However, they nevertheless exhibit certain underlying model-independent commonalities which are relevant for their viability as DDM ensembles. Indeed, these features are identical to those which characterize the "visible" sector of ordinary hadrons, namely

 (i) mass distributions which follow linear Regge trajectories (i.e., $\alpha' M_n^2 \sim n$ where α' is a corresponding Regge slope), and

 (ii) exponentially growing ("Hagedorn-like") degeneracies of states (i.e., $g_n \sim e^{\sqrt{n}} \sim e^{\sqrt{\alpha'} M_n}$).

These features—especially the appearance of an *exponential* scaling of the state degeneracies with mass—represent a behavior which is markedly different from that exhibited by DDM ensembles with polynomial scaling relations. For example, as a result of their exponentially growing densities of states, such ensembles have a critical temperature [12] beyond which their partition functions diverge.

In this paper, we shall study the generic properties of DDM ensembles which exhibit the two features itemized above. We shall calculate the effective equations of state $w_{\text{eff}}(t)$ for such ensembles, and subject these ensembles to those immediate model-independent observational constraints that follow directly from these equations of state. We shall therefore be able to place zeroth-order model-independent bounds on some of the quantities that parametrize these features, such as the effective Regge slope as well as the rate of exponential growth in the state degeneracies. Our primary motivation is to understand the phenomenology that might apply to strongly-coupled dark sectors in their confined ("hadronic") phase, imagining nothing more than that our DDM ensemble resembles the visible hadronic sector in the two respects itemized above. However, the results of such analyses might also be useful in constraining the bulk sector of various classes of string theories, since these bulk sectors also give rise to ensembles of dark-matter states which share these two grossest features. We shall therefore aim to keep our discussion as model-independent as possible, subject to our assumption of the above two properties itemized above. In this way, our analysis and the constraints we obtain can serve as useful phenomenological guides in eventually building realistic dark-matter models of this type.

This paper is organized as follows. In Sec. II, we begin by reviewing the properties that we shall assume for the mass spectrum and density of states of our DDM dark "hadron" ensemble. We shall also discuss the physical interpretations of these properties in terms of a variety of underlying flux-tube models and string theories. This section will also serve to establish our conventions and notation. Then, in Sec. III, we discuss how the required balancing between lifetimes and abundances naturally arises for such DDM ensembles. In particular, we examine the mechanism through which primordial abundances for these hadron resonances are generated, and we determine how these abundances scale across the ensemble as a function of the hadron mass. We also discuss the scaling behavior of the decay widths that characterize the decays of the hadronic ensemble constituents to SM states, as well as the assumptions that enter into such calculations. In Sec. IV, we then derive expressions for the total abundance $\Omega_{\text{tot}}(t)$, the tower fraction $\eta(t)$, and the effective equation-of-state parameter $w_{\text{eff}}(t)$ for these DDM ensemble as functions of time. As discussed in Refs. [1,2] and reviewed in Sec. IV,

these three functions characterize the time evolution of DDM ensembles and allow us to place a variety of general, model-independent constraints on such ensembles. In Sec. V, we then present the results of our analysis of the phenomenological viability of such DDM ensembles, identifying those regions of the corresponding parameter space which lead to the most promising ensembles and uncovering generic phenomenological behaviors and correlations across this space. One of our key findings is that these DDM ensembles can satisfy our constraints across a broad range of energy scales ranging from the GeV scale all the way to the Planck scale, but that the present-day cosmological abundance of the dark sector must be distributed across an increasing number of different states in the ensemble as the fundamental mass scales associated with the ensemble are dialed from the Planck scale down to the GeV scale. Finally, in Sec. VI, we summarize our results and discuss possible avenues for future work.

II. DDM ENSEMBLES OF DARK HADRONS: FUNDAMENTAL ASSUMPTIONS

As discussed in the Introduction, in this paper we are primarily concerned with the properties of DDM ensembles whose constituents are the "hadronic" composite states or resonances of a strongly-coupled dark sector. As has been well known since the 1960s, many of the attributes of such an ensemble can be successfully modeled by strings. These attributes include linear Regge trajectories, linear confinement, an exponential rise in hadron-state degeneracies, and s- and t-channel duality. It is not a complete surprise that there is a deep connection between hadronic spectroscopy and the spectra of string theory. Hadronic resonances (particularly mesons) can be viewed as configurations of dark "quarks" linked together by flux tubes. The spectrum of excitations in such a theory therefore corresponds to the spectrum of fluctuations of these flux tubes. However, it is well known that these flux tubes can be modeled as noncritical strings. Thus string theory can provide insight into the properties of such collections of composite states.

In what follows, we shall use this analogy between hadronic physics and string theory to motivate our parametrization for the mass spectrum and for the density of states of our dark-"hadronic" DDM ensembles. We shall also make recourse to modern string technology, when needed, for refinements of our basic picture. Throughout, however, we shall attempt to keep our parametrizations as general as possible so that they might apply to the widest possible set of DDM ensembles sharing these properties. As discussed in the Introduction, this will allow our analysis and eventual constraints to serve as useful guides in future attempts to build realistic models exhibiting these features.

A. The mass spectrum: Regge trajectories

The first feature that we shall assume of our hadronic dark sector is a mass spectrum consistent with the existence of Regge trajectories. The existence of such trajectories follows directly from nothing more than our assumption that our dark-sector bound states can be modeled by dark quarks connected by the confining flux tube associated with a strong, attractive, dark-sector interaction. Taking meson-like configurations as our guide and temporarily assuming massless quarks, it can easily be shown that the mass M_n associated with a relativistic rotating flux tube scales with the corresponding total angular momentum n as $n \sim \alpha' M_n^2$, where α' is the so-called Regge slope. In the visible sector, this successfully describes the so-called leading Regge trajectory of the observed mesons, with $\alpha' \sim 1 \ (\mathrm{GeV})^{-2}$ appropriate for QCD. Moreover, there also exist subleading (parallel) Regge trajectories of observed mesons which have the same Regge slope but different intercepts: $n \sim \alpha' M_n^2 + \alpha_0$.

Regge trajectories of this form, both leading and subleading, also emerge in string theory. For example, the perturbative states of a quantized open bosonic string have masses M and spins $J = 0, 1, \ldots, J_{\max}$ which satisfy $J_{\max} = \alpha' M^2 + 1$ where α' is now the Regge slope associated with string theory [typically assumed to be $\sim (M_{\mathrm{Planck}})^{-2}$]. The states with $J = J_{\max}$ thus sit along the leading Regge trajectory, while those with smaller values of J sit along the subleading Regge trajectories. Similar results also hold for superstrings and heterotic strings.

Given these observations, in this paper we shall assume that the states of our dark "hadronic" DDM ensemble have discrete positive masses M_n of the general form

$$M_n^2 = n M_s^2 + M_0^2, \qquad (2.1)$$

where n is an index labeling our states in order of increasing mass. Here $M_s \equiv 1/\sqrt{\alpha'}$ is the corresponding "string scale," while M_0 represents the mass of the lightest "hadronic" constituent in the DDM ensemble. Indeed, since we do not expect to have any tachyonic states in our DDM ensemble, we shall assume throughout this paper that $M_0^2 \geq 0$. We shall avoid making any further assumptions about the nature of the dark sector by treating both M_s and M_0 as free parameters to be eventually constrained by cosmological data.

Our choice of sign for M_0^2 perhaps deserves further comment. For the visible sector, most hadrons lie along Regge trajectories with $M_0^2 \geq 0$. While there do exist Regge trajectories with $M_0^2 < 0$, the lowest states in such trajectories are of course absent. In string theory, by contrast, all Regge trajectories have $M_0^2 < 0$. However, just as in the hadronic case, all tachyonic states which might result for small n are ultimately removed from the string spectrum by certain "projections" which are ultimately required for the self-consistency of the string. In other words, for Regge trajectories with $M_0^2 < 0$, one could equivalently relabel our remaining states by shifting $n \rightarrow n - 1$ and thereby obtain an "effective" $M_0^2 \geq 0$. This is not normally done in

string theory because in string theory the index n is correlated with other physical quantities such as the spin of the state. However we are making no such assumption for the states of our dark sector, and are treating the index n as a mere labelling parameter. Our assumption of a tachyon-free dark sector then leads us to take $M_0^2 \geq 0$.

There is also another motivation for taking $M_0^2 \geq 0$. All of the above results which treat n as an angular momentum assume massless quarks at the endpoints of the flux tube. However, while such an approximation holds well for the lightest states in the visible sector, we do not wish to make such an approximation for our unknown dark sector. We shall therefore assume $M_0^2 \geq 0$ in what follows, recognizing that this parameter may in principle also implicitly include the positive contributions from dark quark masses as well.

B. Degeneracy of states: Exponential behavior

The second generic feature associated with hadronic spectroscopy is the well-known exponential rise in the degeneracies of hadrons as a function of mass: $g_n \sim e^{\sqrt{n}}$. This behavior was first predicted and observed for hadrons (both mesons and baryons) in Ref. [12], and also holds as a generic feature for both bosonic and fermionic states in string theory [13].

In general, we can understand this behavior as follows. If we model our hadrons as quarks connected by flux tubes, the degeneracy g_n of hadronic states at any mass level n can be written as the product of two contributions: one factor κ representing a multiplicity of states due to the degrees of freedom associated with the quarks (such as the different possible configurations of quantities like spin and flavor), and a second factor $\hat{g}_n$ representing the multiplicity of states due to the degrees of freedom associated with the flux tube. We thus have

$$g_n \approx \kappa \hat{g}_n. \tag{2.2}$$

While κ is a constant which is independent of the particular mass level n, the remaining degeneracy factor $\hat{g}_n$ counts the rapidly increasing number of ways in which a state of given total energy n can be realized as a combination of the vibrational, rotational, and internal excitations of the different harmonic oscillators which together comprise a quantized string. It is this quantity which grows exponentially with mass, and in string theory the leading behavior of $\hat{g}_n$ for large n generally takes the form [13]

$$\hat{g}_n \approx A n^{-B} e^{C\sqrt{n}} \quad \text{as } n \to \infty, \tag{2.3}$$

where A, B, C are all positive quantities which depend on the particular type of string model under study. Indeed, for any B and C, it turns out that the proper normalization for $\hat{g}_n$ in string theory is given by

$$A = \frac{1}{\sqrt{2}} \left(\frac{C}{4\pi} \right)^{2B-1}. \tag{2.4}$$

Thus our asymptotic degeneracy of states is parametrized by two independent quantities B and C, and we shall assume that this continues to be true in our dark sector as well.

The most salient property of the expression in Eq. (2.3) is that it rises exponentially with $\sqrt{n}$, or equivalently with the mass M_n of the corresponding state. This represents a crucial difference relative to the KK-inspired DDM ensembles previously considered in Refs. [1,2,9] (or even the purely four-dimensional DDM ensembles considered in Refs. [10,11]). For example, the KK states corresponding to a single flat extra spacetime dimension have degeneracies $\hat{g}_n$ which are constant, or which become so above the $n = 0$ level. The key difference here is that the degrees of freedom associated with our flux tube consist of not only KK excitations (if the flux tube happens to be situated within a spacetime with a compactified dimension), but also so-called *oscillator* excitations representing the internal fluctuations of the flux tube itself. It is these oscillator excitations which give rise to the exponentially growing degeneracies and which are a direct consequence of the nonzero spatial extent of the flux tube. As such, they are intrinsically stringy and would not arise in theories involving fundamental point particles.

Unfortunately, the asymptotic form in Eq. (2.3) is not sufficient for our purposes. Although we are interested in the behavior of all states across the DDM ensemble, it is the lighter states rather than the heavier states which are most likely to have longer lifetimes and therefore greater cosmological abundances. Thus, even though we want to keep track of all of the states in our ensemble, we need to be particularly sensitive to the degeneracies of the lighter states, i.e., the states with smaller values of n. This poses a problem because the asymptotic expression in Eq. (2.3) is fairly accurate in the large-n limit but is not especially accurate in the small-n limit.

Fortunately, for values of B and C which correspond to self-consistent strings (to be discussed below), the tools of modern string technology (specifically conformal field theory and modular invariance) furnish us with a more precise approximation for $\hat{g}_n$ which remains accurate even for very small values of n. This expression is given by [14–17]

$$\hat{g}_n \approx 2\pi \left(\frac{16\pi^2 n}{C^2} - 1 \right)^{\frac{1}{4}-B} I_{|2B-\frac{1}{2}|} \left(C \sqrt{n - \frac{C^2}{16\pi^2}} \right), \tag{2.5}$$

where $I_\nu(z)$ denotes the modified Bessel function of the first kind of order ν. Use of the approximation $I_\nu(z) \approx e^z / \sqrt{2\pi z}$ for $z \gg 1$ then reproduces the result in Eq. (2.3). However, the expression in Eq. (2.5) remains valid to within only a few percent all the way down to $n = 1$, assuming $C \leq 4\pi$ (so that the argument of the Bessel function remains real even for $n = 1$).

In what follows, we therefore shall adopt the expression in Eq. (2.5) as our general parametrization for the degeneracy of states $\hat{g}_n$ for arbitrary values of B and $C \leq 4\pi$ and for all $n \geq 1$. For values of B and C corresponding to bonafide string theories, this expression yields results for the state degeneracies which, though not necessarily integral, are highly accurate for all values of $n \geq 1$. An explicit example of this will be provided below. More generally, however, this expression is smooth and well-behaved for all values of the B and C parameters, and in all cases exhibits the exponential Hagedorn-like behavior whose primary effects we seek to analyze in this paper. For $n = 0$, by contrast, we shall define $\hat{g}_0 \equiv 1$, representing the unique ground state of our flux tube.

C. Physical interpretation of ensemble parameters

Thus far we have introduced four parameters to describe our dark "hadron" DDM ensemble: M_s, M_0, B, and C. The first two parameters have immediate interpretations: M_0 is the mass of the lightest state in the DDM ensemble, while M_s parametrizes the splitting between the states. We would now like to develop analogous physical interpretations of B and C.

Clearly B and C describe the dynamics of the flux tube. However, in the case of the ordinary strong interaction, many possible theories governing this dynamics have been proposed. These range from early examples such as the scalar (Nambu) string [18], the Ramond string [19], and the Neveu-Schwarz (NS) string [20] to more modern examples such as Polyakov's "rigid string" [21], Green's "Dirichlet string" [22], and the Polchinski-Strominger "effective string" [23]. Many other possibilities and variants have also been proposed.

All of these theories begin by imagining a one-dimensional line of flux energy (i.e., a string) which sweeps out a two-dimensional flux-sheet (or worldsheet) as it sweeps through an external D-dimensional spacetime. Here D is the number of spacetime dimensions which are effectively uncompactified with respect to the fundamental energy scale M_s associated with the flux tube. As such, as it propagates, our string/flux tube is free to fluctuate into any of the $D_\perp \equiv D - 2$ spatial dimensions transverse to the string. We can describe such fluctuations by specifying $D_\perp$ embedding functions $X^i(\sigma_1, \sigma_2)$, $i = 1, .., D_\perp$, which are nothing but the transverse spacetime locations of any point on the flux-tube worldsheet with coordinates (σ_1, σ_2). As such, these embedding functions may be regarded as fields on the two-dimensional flux-tube worldsheet. The dynamics of this system is then governed by the Polyakov action

$$S \sim M_s^2 \int d^2\sigma \sum_{i=1}^{D_\perp} \left(\frac{\partial}{\partial \sigma^\alpha} X^i \right) \left(\frac{\partial}{\partial \sigma_\alpha} X^i \right). \quad (2.6)$$

Minimizing this action is classically equivalent to minimizing the area of the flux-tube worldsheet.

By itself, the expression in Eq. (2.6) describes the action of the so-called $D_\perp$-dimensional "scalar" string. In some sense this theory provides the simplest possible description of a strongly-interacting flux tube, with the term in Eq. (2.6) representing the bare minimum that must always be present for any flux-tube description. The various possible refinements of this basic theory then differ in the extra terms that might be added to this action. Some of these theories mentioned above introduce extra terms which correspond to additional, purely internal degrees of freedom [e.g., additional fields analogous to $X^i(\sigma_1, \sigma_2)$ but without interpretations as the coordinates of uncompactified spacetime dimensions] on the flux-tube worldsheet. By contrast, other theories introduce extra interaction terms for the X^i-fields which alter their short-distance behavior.

The action in Eq. (2.6) can be interpreted as that of a two-dimensional (2D) field theory (where the two dimensions are those of the flux-tube worldsheet), and we immediately see that it is endowed with a 2D conformal symmetry. There are good reasons to expect that the long-distance limit of any self-consistent flux-tube theory should exhibit such a symmetry, since we expect the physics of this system to be invariant under reparametrizations of our flux-tube worldsheet coordinates. As a result, those flux-tube theories that augment the scalar string by introducing extra purely internal degrees of freedom on the flux-tube worldsheet must not break this conformal symmetry; this requirement constrains what kinds of terms can be added. By contrast, the theories that introduce extra interaction terms for the X^i fields do break this conformal symmetry, but they do so only in the short-distance limit. The 2D conformal symmetry of the long-distance limit is then preserved as an effective symmetry.

In any 2D conformal field theory, either exact or effective, the total number of degrees of freedom is encoded within the so-called *central charge* c. Each X^i field contributes a central charge $c = 1$, and thus the minimal scalar-string action in Eq. (2.6) describes a theory with central charge $c = D_\perp$. However the introduction of additional degrees of freedom on the flux-tube worldsheet will necessarily increase the central charge, producing a theory with $c > D_\perp$.

Given a particular action for our flux-tube dynamics, it is straightforward to quantize the fields in question. In this way, we can determine the corresponding spectrum of the theory at all mass levels. These calculations are standard in string theory (see, e.g., Ref. [13]), and ultimately one obtains [15–17] asymptotic state degeneracies $\hat{g}_n$ of the forms given in Eq. (2.3) or Eq. (2.5). Remarkably, one finds a relatively straightforward connection between the parameters (B, C) appearing in our state degeneracies and the parameters $(D_\perp, c)$ of our underlying flux-tube theory [14–17]:

$$\begin{cases} B = \frac{1}{4}(3 + D_\perp) \\ C = \pi\sqrt{2c/3}. \end{cases} \quad (2.7)$$

Indeed, for any value of B and C, we may regard the total central charge c as having two contributions: one contribution $c_{\text{fluc}} = D_\perp$ associated with the degrees of freedom associated with the transverse uncompactified spacetime fluctuations of the flux tube, and a remaining contribution

$$c_{\text{int}} \equiv c - D_\perp \equiv \frac{3C^2}{2\pi^2} - 4B + 3 \qquad (2.8)$$

associated with those additional, purely internal degrees of freedom which might also exist within the full flux-tube theory (including those associated with any *compactified* spacetime dimensions which may also exist).

At first glance, it might seem that our dark sector must have $D_\perp = 2$, just as does our visible sector. This would certainly be true if our dark-sector flux tube were to experience the same spacetime geometry as does the visible sector. However, we emphasize that in a string-theoretic or "braneworld" context, the dark sector could correspond to physics in the "bulk"—i.e., physics perpendicular to the brane on which the visible sector resides. The degrees of freedom in the bulk would then be able to interact with those on the brane at most gravitationally, and would thus constitute dark matter by construction. However, the geometric properties of the bulk will generally differ from those of the brane—the bulk might contain not only extra spacetime dimensions which are effectively large (i.e., uncompactified) with respect to the fundamental string scale, but also extra spacetime dimensions which are small (i.e., compactified). The bulk may also be populated by additional fields with no spacetime interpretations at all. It is for this reason that we make no assumptions about the values of c or $D_\perp$ associated with the dark sector.

Once our flux-tube theory is specified and the corresponding values of B and C determined, we may calculate the corresponding effective static-quark potential $V(R)$ between two quarks a distance R apart. We find [14]

$$V(R) = \left(\frac{M_s}{2\pi}\right)\sqrt{(M_s R)^2 - (C/2)^2}$$

$$\approx \frac{M_s^2 R}{2\pi} - \frac{C^2}{16\pi}\frac{1}{R} + \cdots \quad \text{for } R \gg M_s^{-1}. \qquad (2.9)$$

The first term in the final expression indicates a linear confinement potential, as expected; this is nothing but the classical energy in the flux tube. By contrast, the second term resembles a Coulomb term but is actually an attractive universal quantum correction (or Casimir energy) which arises due to the transverse zero-point vibrations of the flux tube.

For visible-sector hadrons, it is natural to take $D = 4$. As a result, the $D_\perp = 2$ scalar string with $c_{\text{int}} = 0$ (corresponding to $B = 5/4$ and $C = 2\pi/\sqrt{3} \approx 3.63$) is the "minimal" string that we expect to underlie all descriptions of the actual visible-sector QCD flux tube. In fact, it has

been shown in Ref. [14] that this minimal $D_\perp = 2$ scalar string with $\kappa = 36$ provides an excellent fit to hadronic data, both for low energies (which are sensitive to the Casimir energy within the confinement potential) as well as high energies (which are governed by the asymptotic degeneracy of hadronic states and the corresponding Hagedorn temperature). As discussed in Ref. [14], this success—coupled with the appearance of the same quantity C in both places—provides a highly nontrivial test of the classical conformal invariance of the QCD string.

In this paper, we shall imagine that our DDM ensemble of dark-sector hadrons mimics that of the visible-sector hadrons to the extent that it corresponds to a set of masses M_n and state degeneracies $\hat{g}_n$ parametrized by the functional forms given in Eqs. (2.1) and (2.5). However, we shall not insist on an actual string interpretation governing our dark-sector confinement dynamics, and as discussed above we shall therefore regard B and C as free parameters which may be adjusted at will (subject to certain constraints to be discussed below). Nevertheless it is only when B and C correspond to appropriate values of $D_\perp$ and c via the relations in Eq. (2.7) that we may describe our resulting spectrum as corresponding to that of a classically self-consistent string moving in a specific geometry. Moreover, motivated by our experience with visible-sector hadrons, we shall continue to regard the special scalar-string case with $B = 5/4$ and $C = 2\pi/\sqrt{3}$ as our "minimal" theory, corresponding to the action in Eq. (2.6) with $D_\perp = 2$. Adjusting the value of B above or below $5/4$ can then be interpreted as changing the effective number of uncompactified spacetime dimensions felt by our dark-sector flux tube (i.e., the number of uncompactified spacetime dimensions into which it can experience fluctuations), while increasing the value of C beyond $2\pi/\sqrt{3}$ corresponds to introducing additional purely internal degrees of freedom with central charge c_{int} into our flux-tube theory.

Note, in this regard, that the degrees of freedom associated with fluctuations into extra *compactified* spacetime dimensions count towards c_{int} rather than $D_\perp$. Thus, in terms of its effects on the dark sector, the act of compactifying a spacetime dimension to a radius below the associated string scale preserves the central charge c (and thus the coefficient C) and merely shifts the associated degrees of freedom from $D_\perp$ to c_{int}. The resulting change in the asymptotic state degeneracies $\hat{g}_n$ due to the change in B then reflects the appearance of new Kaluza-Klein resonances in the total flux-tube spectrum.

D. Constraints on parameters

Even though M_s, M_0, B, and C are henceforth to be viewed as unrestricted quantities parametrizing our hadronlike DDM ensemble, they are nevertheless subject to certain self-consistency constraints.

First, we note that while the asymptotic form for $\hat{g}_n$ in Eq. (2.5) is remarkably accurate within those regions of

(B, C) parameter space for which actual string realizations exist, there are other regions of (B, C) parameter space within which this approximation provides unphysical results. For example, given that the expression for $\hat{g}_n$ in Eq. (2.5) multiplies a growing Bessel function against a falling monomial, for any given value of B it is in principle possible for there to exist a critical value of C below which $\hat{g}_n$ is not always monotonically increasing for all $n \geq 0$. Such a situation is clearly unphysical, implying that the number of accessible flux-tube states fails to grow with the total energy in the flux tube. We therefore demand that

$$\hat{g}_{n+1} > \hat{g}_n \quad \text{for all } n \geq 0. \tag{2.10}$$

Given that we have taken $\hat{g}_0 = 1$, it turns out throughout the parameter range of interest that this requirement is tantamount to demanding

$$\hat{g}_1 > 1. \tag{2.11}$$

If we further wish to demand that our ensemble of dark "hadrons" admit a string-theoretic description, then certain additional consistency conditions on the parameters B and C must be satisfied as well. For example, since $D_\perp \in \mathbb{Z} > 0$ in any self-consistent string construction, we must have

$$B \in \mathbb{Z}/4 > 3/4. \tag{2.12}$$

Likewise, as discussed above, any self-consistent string theory will also have $c \geq D_\perp$ (or $c_{\text{int}} \geq 0$), which in turn implies

$$C^2 \geq \frac{2\pi^2}{3}(4B - 3). \tag{2.13}$$

There are, of course, further string-derived constraints that might be imposed. For example, the allowed set of worldsheet central charges c that can be realized in such noncritical string theories depends crucially on the types of string models under study and the types of conformal field theories used in their constructions. However, the constraints in Eqs. (2.12) and (2.13) can be taken as a minimal model-independent set of constraints that must be satisfied as a prerequisite to any possible string interpretation.

In Fig. 1, we indicate the region of (B, C) parameter space which is consistent with the constraints in Eqs. (2.11), (2.12), and (2.13). We emphasize that the first of these constraints must always be satisfied as a matter of internal self-consistency. By contrast, as discussed above, the latter two conditions need to be satisfied only if one imposes the additional stipulation that our ensemble of dark "hadrons" admit a string-theory description. We observe in this connection that the first constraint is always weaker than the remaining string-motivated constraints. In other words, a string-based description with $B \in \mathbb{Z}/4 \geq 1$ is always guaranteed to have monotonically growing degeneracies $\hat{g}_n$. In Fig. 1 we also highlight the point $(B, C) = (5/4, 2\pi/\sqrt{3})$ corresponding to the "minimal" $D_\perp = 2$
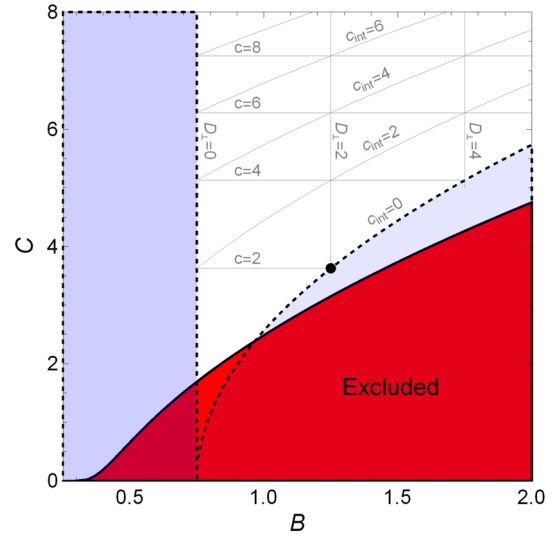

FIG. 1. The region of (B, C) parameter space of interest for a DDM ensemble of dark "hadrons." The red shaded region is excluded by the theoretical self-consistency condition $\hat{g}_1 \geq 1$. By contrast, the blue shaded regions are excluded by the constraint $B > 3/4$ as well as by the constraint in Eq. (2.13), and thus correspond to regions in which it would not be possible to interpret the ensemble constituents as the states of a quantized string. Note that locations for which $B \notin \mathbb{Z}/4$ would also suffer from this difficulty. Within the (unshaded) string-allowed region, we have indicated contours of $D_\perp$, c, and c_{int}, as defined in Eqs. (2.7) and (2.8). The black dot indicates the point in parameter space corresponding to the minimal $D_\perp = 2$ scalar string with $c_{\text{int}} = 0$. As demonstrated in Ref. [14], this model provides the best fit to the visible hadron spectrum.

scalar string. While this theory need not necessarily provide the best-fit description for our dark hadrons (as it does for the visible hadrons), its minimality nevertheless provides a useful benchmark for exploring the parameter space of our DDM model. Finally, we observe from Fig. 1 that our combined constraints imply that

$$C \gtrsim 1.693. \tag{2.14}$$

Indeed, this is the allowed range in C for which $\hat{g}_1 > 1$ when $B = 3/4$.

As an illustration of the results of this section, let us focus further on this "minimal" $D_\perp = 2$ scalar string. As noted above, the action for this string is given in Eq. (2.6). Quantizing this theory then gives rise to a discrete spectrum of states whose exact degeneracies are[1] $\hat{g}_{n \geq 0} = \{1, 2, 5, 10, 20, 36, 65, 110, 185, \ldots\}$. Indeed it is only

---

[1] These degeneracies $\hat{g}_n$ may be extracted as the coefficients of q^n in a small-q power-series expansion of the infinite product $\prod_n (1 - q^n)^{-2}$. With only minor modifications and a proper physical definition for q, this infinite product turns out to be the partition function of the $D_\perp = 2$ scalar string theory in Eq. (2.6).
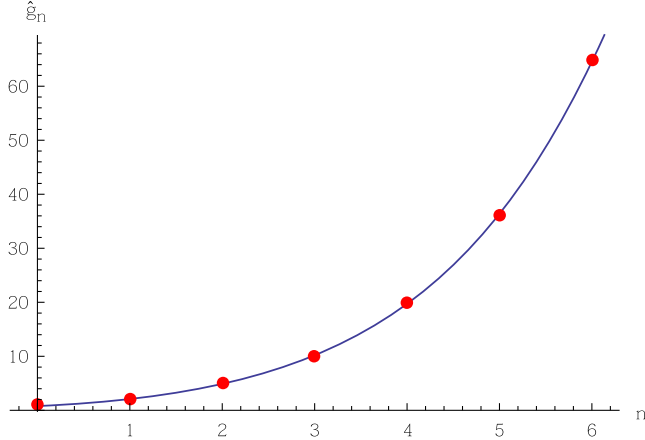
FIG. 2. State degeneracies $\hat{g}_n$ for the $D_\perp = 2$ scalar-string flux-tube model of Eq. (2.6) (red circles), with the asymptotic functional form in Eq. (2.5) superimposed (blue line). It is clear that our asymptotic functional form succeeds in modelling the state degeneracies extremely accurately all the way down to the ground state, as we shall require for our analysis.

because of the existence of a quantized string formulation that we are even able to calculate the degeneracies of the corresponding ensemble from first principles. However, as we have asserted, these degeneracies are extremely well approximated by the expression in Eq. (2.5) with $(B, C) = (5/4, 2\pi/\sqrt{3})$. This is shown in Fig. 2, where we plot both the discrete exact degeneracies $\hat{g}_n$ and the approximate functional form in Eq. (2.5). As evident from Fig. 2, our functional form matches these discrete values of $\hat{g}_n$ extremely well for all values of $n \geq 0$—even though the degeneracies $\hat{g}_n$ are necessarily integers and even though our functional form was originally designed to be accurate only in the asymptotic $n \to \infty$ limit. Indeed, as claimed above, this functional form is accurate to within two percent over the entire range of n. This demonstrates the power of the functional form we have adopted, as well as the utility of an underlying string formulation for our flux tube.

III. LIFETIMES AND COSMOLOGICAL ABUNDANCES FOR HADRONIC DDM ENSEMBLES

In the previous section, we discussed the spectra of our dark "hadronic" DDM ensembles. Our next step, then, is to consider the lifetimes and cosmological abundances of the individual states within these ensembles.

A. Cosmological abundances

As we have seen, the degeneracy of states g_n for our ensemble of dark "hadrons" grows exponentially with the mass of the state, with asymptotic behavior $g_n \sim e^{\sqrt{n}} \sim e^{M_n/M_s}$. This exponential rise in the state degeneracies places severe constraints on the possible, physically consistent cosmological production mechanisms by which the

corresponding abundances Ω_n might be established. Indeed, unless the corresponding abundances Ω_n fall sufficiently rapidly with n, our ensemble is likely to encounter severe phenomenological difficulties.

Fortunately, our interpretation of the individual components of such an ensemble as dark hadrons suggests a natural mechanism through which the corresponding abundances Ω_n are generated with an exponential suppression factor capable of overcoming this exponential rise in g_n. As we have discussed, we have been imagining that these dark "hadrons" emerge as the result of a dark-sector confining phase transition triggered by the strong interactions of some dark-sector gauge group G. This phase transition occurs when the temperature T in the dark sector drops below the critical temperature T_c associated with this phase transition. This event marks the time t_c at which the primordial abundances of our individual hadrons are established. Moreover, it is reasonable to assume that residual G interactions establish thermal equilibrium among these hadrons at $T \sim T_c$. Thus, the primordial abundances Ω_n of our hadrons can be assumed to follow a Boltzmann distribution at $t = t_c$:

$$\Omega_n(t_c) \equiv \frac{\rho_n(t_c)}{\rho_{\mathrm{crit}}(t_c)} = \frac{1}{3\tilde{M}_P^2 H(t_c)^2} \int \frac{d^3\mathbf{p}}{(2\pi)^3} E_\mathbf{p} e^{-E_\mathbf{p}/T_c} \quad (3.1)$$

where $E_\mathbf{p} \equiv \sqrt{\mathbf{p} \cdot \mathbf{p} + M_n^2}$ and $\rho_{\mathrm{crit}}(t) \equiv 3\tilde{M}_P^2 H(t)^2$ where $\tilde{M}_P \equiv M_P/\sqrt{8\pi} = 1/\sqrt{8\pi G_N}$ is the reduced Planck mass and $H(t)$ the Hubble parameter. Indeed, we may equivalently regard these abundances as emerging from an infinitely rapid succession of thermal freeze-outs. Evaluating Eq. (3.1) explicitly, we find

$$\Omega_n(t_c) = X\left\{ (M_n T_c)^2 K_2(M_n/T_c) \right.$$
$$\left. + \frac{1}{2} M_n^3 T_c [K_1(M_n/T_c) + K_3(M_n/T_c)] \right\} \quad (3.2)$$

where $K_\nu(z)$ are modified Bessel functions of the second kind and where $X \equiv [6\pi^2 \tilde{M}_P^2 H(t_c)^2]^{-1}$ is a common overall multiplicative factor.

In general, a given state with mass M produced at temperature T_c will be nonrelativistic (behaving like massive matter) if $T_c \lesssim M$ and relativistic (behaving like radiation) otherwise. In such limiting cases, the abundances in Eqs. (3.1) and (3.2) take the simplified forms

$$\Omega_n(t_c) \approx \begin{cases} \sqrt{\pi/2} X M_n (M_n T_c)^{3/2} e^{-M_n/T_c} & \text{nonrel} \\ 6X T_c^4 & \text{rel.} \end{cases} \quad (3.3)$$

At first glance, it may seem that any value for T_c might be phenomenologically permissible. However, this production mechanism can only be self-consistent if it injects a finite total energy density into our system. In other words, as a bare minimum, we must require that

$$\Omega_{\rm tot}(t_c) \equiv \sum_{n=0}^{\infty} g_n \Omega_n(t_c) < \infty. \qquad (3.4)$$

However, this condition is sensitive to the behavior of the abundances $\Omega_n(t_c)$ for extremely large n, corresponding to states which are nonrelativistic. For such states, we see from Eq. (3.3) that $\Omega_n(t_c) \sim e^{-M_n/T_c}$. With $g_n \sim n^{-B} e^{C\sqrt{n}}$ as $n \to \infty$, we find using Eqs. (2.1) and (3.1) that Eq. (3.4) can only hold if

$$\frac{T_c}{M_s} \leq \frac{1}{C}. \qquad (3.5)$$

This then becomes a hard bound on the allowed values of T_c, one which ensures that the Boltzmann exponential suppression factor in Eq. (3.1) ultimately overcomes the exponential rise in the degeneracy of states g_n. Indeed, Eq. (3.5) reflects nothing more than the statement that $T_c \leq T_H$, where $T_H \equiv M_s/C$ is the Hagedorn temperature of our dark ensemble. For the *visible* hadronic sector, one often assumes that T_c and T_H are related to each other parametrically, with T_c either directly identified as T_H or positioned not too far below T_H. We shall implicitly make the same assumption for the dynamics of our dark sector as well.

The next question is to determine which of our ensemble components are produced relativistically or nonrelativistically at $T = T_c$. To do this, we shall henceforth assume that $T_c, M_s, M_0 > T_{\rm MRE}$ where $t_{\rm MRE}$ and $T_{\rm MRE}$ are the time and temperature associated with matter-radiation equality. This assumption, which parallels what occurs for the hadrons of the visible sector, ensures that our abundances $\Omega_n(t)$ are established during the radiation-dominated era prior to matter-radiation equality and that all ensemble constituents have become effectively nonrelativistic by $t_{\rm MRE}$. Note that the assumption that $T_c > T_{\rm MRE}$ follows from our expectation that our dark degrees of freedom prior to t_c (i.e., prior to "hadronization" in the dark sector) are likely to be relativistic, thereby reinforcing the radiation-dominated nature of the era prior to $T_{\rm MRE}$ and making matter-radiation equality impossible to achieve using only visible-sector matter, as would have been required had we taken $T_c < T_{\rm MRE}$. Similarly, the assertion that $M_s > T_c$ follows directly from our assumption that $T_c > T_{\rm MRE}$, given the constraints in Eqs. (2.14) and (3.5). Finally, although it is not impossible to imagine self-consistent scenarios in which $M_0 < T_{\rm MRE}$, taking $M_0 > T_{\rm MRE}$ also helps to preserve $t_{\rm MRE}$ at its standard cosmological value. We shall nevertheless make no assertion regarding the relative sizes of M_0 and T_c.

The above assumptions enable us to determine which of the components of our ensemble are relativistic or nonrelativistic at $T = T_c$. To do this, we simply compare T_c against the ensemble masses M_n given in Eq. (2.1). Given the constraint in Eq. (3.5), it is straightforward to demonstrate that

$$T_c \leq \frac{M_s}{C} \leq \frac{M_1}{C}. \qquad (3.6)$$

Since $C > 1$ [as follows from Eq. (2.14)], we conclude that *all of our ensemble components with $n \geq 1$ are necessarily nonrelativistic at $t = t_c$*. By contrast, the $n = 0$ component will be relativistic at $t = t_c$ if $T_c \gtrsim M_0$, and nonrelativistic otherwise.

Equation (3.1) describes the abundances of our dark-sector hadrons at the time t_c when these hadrons come into existence as the result of a dark-sector confining transition. However, once established, these abundances then evolve nontrivially with time as a result of two effects. The first of these is Hubble expansion; the second is particle decay. We shall treat each of these effects separately.

In order to evaluate the effect of Hubble expansion on the abundances $\Omega_n(t)$, we shall assume a standard cosmological history in which the universe remains radiation-dominated (RD) from very early times up to the time $t_{\rm MRE}$ of matter-radiation equality. We shall also approximate the universe as matter-dominated (MD) throughout the subsequent epoch. In general, we recall that the abundance $\Omega(t)$ of nonrelativistic matter scales as $t^{1/2}$ during an RD epoch but remains constant in an MD epoch; by contrast, the abundance of relativistic matter remains constant during an RD epoch but scales as $t^{-2/3}$ during an MD epoch. Likewise, we recall that the temperature T of the universe scales as $T \sim t^{-1/2}$ during RD but $T \sim t^{-2/3}$ during MD. Thus any ensemble component of mass M which is "born" relativistic at $T = T_c \gg M$ will eventually transition to nonrelativistic behavior as the temperature ultimately drops below $T \sim M$.

Collecting these observations, we then find that the net effect of Hubble expansion is to rescale the original abundance of a given state of mass M by a factor which depends on whether that state was nonrelativistic or relativistic at the time t_c of its production:

$$\Omega(t) = \Omega(t_c) \times \begin{cases} \sqrt{t_{\rm MRE}/t_c} & {\rm nonrel} \\ \sqrt{t_{\rm MRE}/t_M} & {\rm rel} \end{cases} \qquad (3.7)$$

where t_M denotes the time at which $T = M$. Note that this result is valid for any time $t \geq t_{\rm MRE}$. Since it follows from our assumptions that $t_c, t_M < t_{\rm MRE}$, we see that the abundances of all of our ensemble states are necessarily *enhanced* before reaching the current MD era. However, as evident from Eq. (3.7), these abundances are not enhanced equally: the abundance of a nonrelativistic component is enhanced more greatly than that of any relativistic component of mass M a factor $\sqrt{t_M/t_c}$.

We have already seen that the states with $n \geq 1$ are all nonrelativistic, while the $n = 0$ ground state is either relativistic or nonrelativistic depending on the value of M_0/T_c. Thus, putting all of the pieces together, we find for all $n \geq 1$ that

$$\Omega_n(t) = \sqrt{\frac{\pi}{2}} X M_n (M_n T_c)^{3/2} e^{-M_n/T_c} \sqrt{\frac{t_{\mathrm{MRE}}}{t_c}}$$

$$= \sqrt{\frac{\pi}{2}} X \left(\frac{g_c}{g_{\mathrm{MRE}}}\right)^{1/4} \frac{(M_n T_c)^{5/2}}{T_{\mathrm{MRE}}} e^{-M_n/T_c}$$

$$= \sqrt{\frac{\pi}{72}} \frac{1}{g_c^{3/4} g_{\mathrm{MRE}}^{1/4}} \frac{M_n^{5/2}}{T_c^{3/2} T_{\mathrm{MRE}}} e^{-M_n/T_c}. \qquad (3.8)$$

Note that in passing to the second line we have exploited the standard time/temperature relationship suitable for an RD epoch, specifically[2]

$$t = \sqrt{\frac{\pi}{32}} g_*(T)^{-1/2} \frac{M_P}{T^2}, \qquad (3.9)$$

where $g_*(T)$ tallies the number of effectively relativistic degrees of freedom driving the Hubble expansion at any temperature T, with $g_\alpha \equiv g_*(T_\alpha)$. Likewise, in passing to the final line of Eq. (3.8) we have recognized that $H = 1/(2t)$ for an RD epoch, from which it follows that $X = 1/(6 g_c T_c^4)$.

For $n = 0$, however, the corresponding cosmological abundance is given by

$$\Omega_0(t) = \begin{cases} \sqrt{\frac{\pi}{72}} \frac{1}{g_c^{3/4} g_{\mathrm{MRE}}^{1/4}} \frac{M_0^{5/2}}{T_c^{3/2} T_{\mathrm{MRE}}} e^{-M_0/T_c} & T_c \lesssim M_0 \\[2ex] \frac{1}{g_c} \left(\frac{g_{M_0}}{g_{\mathrm{MRE}}}\right)^{1/4} \left(\frac{M_0}{T_{\mathrm{MRE}}}\right) & T_c \gtrsim M_0. \end{cases}$$

$$(3.10)$$

As expected, the cosmological abundances in Eqs. (3.8) and (3.10) depend nontrivially on the three mass scales which parametrize our dark-hadron mass spectrum, namely M_0, T_c, and M_s (the latter appearing implicitly through M_n). They also depend on the fixed mass scale T_{MRE}. However, if we disregard the numerical g-factors which appear in these results and which only serve to parametrize the external time/temperature relationship, we see that the *ratios* between these abundances depend only on the *ratios* between our input mass scales. In particular, such abundance ratios are no longer anchored to a fixed external mass scale such as T_{MRE}. To make this point explicit, let us define the dimensionless quantities

$$r \equiv \frac{M_0}{M_s} \quad \text{and} \quad s \equiv \frac{T_c}{M_s} \qquad (3.11)$$

and imagine that $g_*(T)^{1/4}$ does not change significantly between T_c and M_0. (Note, indeed, that $g^{1/4}$ varies much

more slowly than g.) We then find from Eqs. (3.8) and (3.10) that

$$\frac{\Omega_{n \geq 1}(t)}{\Omega_0(t)} = \begin{cases} \frac{(n+r^2)^{5/4}}{r^{5/2}} e^{-(\sqrt{n+r^2}-r)/s} & s \lesssim r \\[2ex] \sqrt{\frac{\pi}{72}} \frac{(n+r^2)^{5/4}}{r s^{3/2}} e^{-\sqrt{n+r^2}/s} & s \gtrsim r. \end{cases} \qquad (3.12)$$

Thus, up to an overall rescaling factor Ω_0, we see that all of our abundances Ω_n depend purely on the dimensionless ratios r and s. It then follows that the cosmological abundance of each state in our dark-hadron ensemble is determined once Ω_0 is anchored to a particular numerical value and specific values of r and s are chosen. This observation will be important in what follows.

B. Lifetimes and decays

As indicated above, our derivation of the dark-sector cosmological abundances $\Omega_n(t)$ has thus far disregarded the effects of particle decays. In other words, we have implicitly assumed that each ensemble component is absolutely stable once produced at T_c. As our final step, we shall therefore now incorporate the effects of such decays into our analysis. In doing so, we shall make several simplifying assumptions. First, we shall assume that the net injection of energy density in the form of radiation from these decays has a negligible effect on the total radiation-energy density of the universe. Hence, this effect decouples from the effect of Hubble expansion. Second, we shall further assume that the contribution to the total decay width Γ_n of each ensemble constituent from intra-ensemble decays is negligible. In other words, we shall assume that Γ_n is dominated by decays to visible-sector final states which do not include lighter ensemble constituents. We shall discuss the consequences of relaxing this assumption in Sec. VI. Third, we shall assume that all states at a given mass level n share a common decay width Γ_n, and that this width scales with n across our dark-hadron ensemble according to

$$\Gamma_n = \Gamma_0 \left(\frac{M_n}{M_0}\right)^\xi \qquad (3.13)$$

where M_n are the dark-hadron masses in Eq. (2.1) and where Γ_0 (or, equivalently, the corresponding lifetime τ_0) and the scaling exponent $\xi > 0$ are taken to be additional free parameters of our model. Thus each state in our dark-sector ensemble has a lifetime $\tau_n \equiv 1/\Gamma_n$ given by

$$\tau_n = \tau_0 \left(\frac{n}{r^2} + 1\right)^{-\xi/2}. \qquad (3.14)$$

Finally, for simplicity, we shall imagine that all states with lifetimes τ_n indeed actually decay at $t = \tau_n$.

Under these assumptions, the abundance $\Omega_n(t)$ of any ensemble constituent at any time $t \geq t_c$ is given by the

---

[2]Note that the factor of $\sqrt{\pi/32}$ in Eq. (3.9) is consistent with our adoption of Boltzmann statistics in Eq. (3.1); for Bose-Einstein statistics this would instead become $\sqrt{45/16\pi^3}$.

expressions quoted above, but now multiplied by an additional decay factor

$$e^{-(t-t_c)/\tau_n} \approx e^{-(\sqrt{n+r^2}/r)^\xi(t/\tau_0)} \qquad (3.15)$$

where we have approximated $t \gg t_c$. For $s \lesssim r$, we thus have

$$\Omega_{n\geq 1}(t) = \Omega_0^{(\mathrm{NR})}(t) \frac{(n+r^2)^{5/4}}{r^{5/2}} \mathcal{E}_n^{(\mathrm{NR})}(t) \qquad (3.16)$$

where

$$\mathcal{E}_n^{(\mathrm{NR})}(t) \equiv e^{-(\sqrt{n+r^2}-r)/s-[(\sqrt{n+r^2}/r)^\xi-1]t/\tau_0} \qquad (3.17)$$

and where

$$\Omega_0^{(\mathrm{NR})}(t) = \sqrt{\frac{\pi}{72}} \frac{1}{g_c^{3/4} g_{\mathrm{MRE}}^{1/4}} \left(\frac{r}{s}\right)^{3/2} \left(\frac{M_0}{T_{\mathrm{MRE}}}\right) e^{-r/s-t/\tau_0}. \qquad (3.18)$$

By contrast, for $s \gtrsim r$, we have

$$\Omega_{n\geq 1}(t) = \sqrt{\frac{\pi}{72}} \Omega_0^{(\mathrm{R})}(t) \frac{(n+r^2)^{5/4}}{rs^{3/2}} \mathcal{E}_n^{(\mathrm{R})}(t) \qquad (3.19)$$

where

$$\mathcal{E}_n^{(\mathrm{R})}(t) \equiv e^{-\sqrt{n+r^2}/s-[(\sqrt{n+r^2}/r)^\xi-1]t/\tau_0} \qquad (3.20)$$

and where

$$\Omega_0^{(\mathrm{R})}(t) = \frac{1}{g_c} \left(\frac{g_{M_0}}{g_{\mathrm{MRE}}}\right)^{1/4} \left(\frac{M_0}{T_{\mathrm{MRE}}}\right) e^{-t/\tau_0}. \qquad (3.21)$$

IV. COSMOLOGICAL CONSTRAINTS ON THE DARK-HADRON ENSEMBLE

Having determined the abundances and lifetimes of each of the individual components of our dark-hadron DDM ensemble, we now proceed to study the overall properties of our ensemble and its behavior as a function of time. However, as we shall see, many of the phenomenological properties and constraints that apply to such an ensemble do not rest upon the properties of the individual ensemble components *per se*, but rather upon various aggregate quantities that collectively describe the ensemble as a whole. Accordingly, in this section we shall begin by describing three aggregate quantities which ultimately play the most important roles in characterizing and constraining such dark-hadron DDM ensembles. We shall then discuss of some of the most immediate cosmological constraints that can be placed upon these quantities.

A. Total abundance, tower fraction, and effective equation of state

Perhaps not surprisingly, the first aggregate property of a given dark-hadron DDM ensemble that shall concern us is its total abundance

$$\Omega_{\mathrm{tot}}(t) \equiv \sum_{n=0}^{\infty} g_n \Omega_n(t) = \kappa \sum_{n=0}^{\infty} \hat{g}_n \Omega_n(t). \qquad (4.1)$$

Given our results in Eqs. (3.16) and (3.19), this total abundance takes the form

$$\Omega_{\mathrm{tot}}(t) = \begin{cases} \kappa\Omega_0^{(\mathrm{NR})}(t)\left[1 + \sum_{n=1}^{\infty} \hat{g}_n \frac{(n+r^2)^{5/4}}{r^{5/2}} \mathcal{E}_n^{(\mathrm{NR})}(t)\right] & s \lesssim r \\ \kappa\Omega_0^{(\mathrm{R})}(t)\left[1 + \sqrt{\frac{\pi}{72}} \sum_{n=1}^{\infty} \hat{g}_n \frac{(n+r^2)^{5/4}}{rs^{3/2}} \mathcal{E}_n^{(\mathrm{R})}(t)\right] & s \gtrsim r \end{cases} \qquad (4.2)$$

where $\Omega_0^{(\mathrm{NR,R})}(t)$ are given in Eqs. (3.18) and (3.21). Indeed, we further note from Eqs. (3.18) and (3.21) that

$$\Omega_0^{(\mathrm{NR,R})}(t) = e^{-(t-t_{\mathrm{now}})/\tau_0} \Omega_0^{(\mathrm{NR,R})}(t_{\mathrm{now}}) \qquad (4.3)$$

where $t_{\mathrm{now}} \approx 4 \times 10^{17}$ s denotes the current age of the universe. We thus see from Eqs. (4.2) and (4.3) that the overall magnitude of $\Omega_{\mathrm{tot}}^{(\mathrm{NR,R})}(t)$ can be viewed as being set by the single number $\Omega_0^{(\mathrm{NR,R})}(t_{\mathrm{now}})$.

In characterizing the properties of our DDM ensemble and how they evolve with time, we are certainly interested in tracking $\Omega_{\mathrm{tot}}(t)$. However, we are also interested in tracking the *distribution* of this total abundance among the individual ensemble constituents. One quantity of particular interest that provides essential information about this distribution is the so-called "tower fraction" $0 \leq \eta(t) < 1$ originally introduced in Ref. [1]. This quantity is typically defined in the DDM literature as the fraction of the abundance carried by all ensemble components *other* than the dominant component, where the dominant component is the one making the largest individual contribution to $\Omega_{\mathrm{tot}}(t)$. As such, the quantity η tracks the degree to which a single component carries the bulk of the total abundance. When η is close to zero, our ensemble effectively resembles a traditional single-component dark-matter setup. By contrast, when η differs significantly from zero, our ensemble is more truly "DDM-like," with many of the ensemble

constituents playing a nontrivial role in together shaping the properties of the dark sector.

Such a definition for η is appropriate in cases in which each ensemble constituent has a unique mass and lifetime. Indeed, this has often been the case for the types of DDM ensembles previously studied. However, for the dark-hadron DDM ensembles on which we are focusing here, the states at a given Regge level n have been assumed to have essentially equal masses and lifetimes. Thus, in this paper, we shall adopt a modified definition for $\eta(t)$ in which the comparison is made between the aggregate abundance contributions that accrue *level by level* rather than state by state. Specifically, we define

$$\hat{\Omega}_n(t) \equiv g_n \Omega_n(t) \qquad (4.4)$$

as the aggregate cosmological abundance arising from all states at a particular oscillator level n. In terms of these aggregate abundances, we then define

$$\eta(t) \equiv 1 - \frac{\max_n\{\hat{\Omega}_n(t)\}}{\Omega_{\text{tot}}(t)}. \qquad (4.5)$$

Thus we continue to have $0 \leq \eta(t) < 1$, with $\eta \approx 0$ signifying a dark sector resembling traditional single-component dark matter and $\eta > 0$ indicating (and quantifying) a DDM-like departure from this traditional scenario.

At first glance, one might assume that the $n = 0$ ground state(s) must always yield the largest aggregate abundance $\hat{\Omega}_n(t)$ because the primordial abundances $\Omega_n(t)$ for the states at all higher levels $n > 0$ are exponentially suppressed by the corresponding Boltzmann factor in Eq. (3.1). However, for the DDM ensembles of dark hadrons studied here, it often turns out that the Hagedorn-like exponential growth of the degeneracies g_n as a function of n can more than compensate for the Boltzmann suppression for small values of n. Indeed, this is true even for combinations of the ensemble parameters B, C, r, and s which satisfy the consistency conditions discussed in Sec. II and which yield a finite value of $\Omega_{\text{tot}}(t_c)$. As a result of this net balancing between these two competing exponential effects, the level carrying the greatest aggregate cosmological abundance $\hat{\Omega}_n(t)$ need not always be the $n = 0$ ground state. It need not even be fixed as a function of time. This possibility must therefore be taken into account when evaluating $\eta(t)$.

Finally, another important quantity which can be taken to characterize our dark sector is the so-called equation-of-state parameter w. For a single-component dark sector, this quantity is nothing but the ratio between the pressure p and energy density ρ of the dark component: $p = w\rho$. However, we are dealing here with a multicomponent dark sector in which each component has its own individual lifetime and abundance. As a result, the total energy density and pressure associated with our dark sector will generally experience a rather nontrivial time dependence which

causes our ensemble as a whole to behave collectively as if it had a nontrivial w—even if each individual component is taken to be pure matter with $w = 0$.

To describe these collective effects, we therefore define [1] an *effective* equation-of-state parameter $w_{\text{eff}}(t)$ which describes the behavior of our ensemble as a single collective entity:

$$w_{\text{eff}}(t) \equiv -\left(\frac{1}{3H}\frac{d\log\rho_{\text{tot}}}{dt} + 1\right). \qquad (4.6)$$

Here H is the Hubble parameter and $\rho_{\text{tot}} = 3\tilde{M}_P H^2 \Omega_{\text{tot}}$ is the total energy density of the ensemble. Note that the definition in Eq. (4.6) is nothing but the usual definition of w prior to any assumptions of dark-sector minimality. As discussed above, we are primarily concerned with the evolution of the ensemble during the present matter-dominated epoch, within which $H(t) \approx 2/(3t)$. Thus, the effective equation-of-state parameter for our DDM ensemble within this epoch is given by

$$w_{\text{eff}}(t) = -\frac{t}{2\Omega_{\text{tot}}}\frac{d\Omega_{\text{tot}}(t)}{dt}. \qquad (4.7)$$

As discussed in Sec. III, the only explicit dependence of $\Omega_{\text{tot}}(t)$ on t within a matter-dominated epoch is due to the exponential decay factor (3.15) within each individual abundance $\Omega_n(t)$. We thus find that

$$w_{\text{eff}}(t) = \frac{t}{2\tau_0 \Omega_{\text{tot}}(t)}\sum_{n=0}^{\infty} g_n\left(\frac{\sqrt{n+r^2}}{r}\right)^{\xi}\Omega_n(t). \qquad (4.8)$$

Note that even though each of the individual components of our ensemble has been taken to be matter-like (with $w = 0$), the collective equation-of-state parameter $w_{\text{eff}}(t)$ for our ensemble as a whole is *positive*, reflecting the fact that the ensemble as a whole is continually losing abundance as its individual components decay. Indeed, it is only in the $\tau_0 \to \infty$ limit that $w_{\text{eff}}(t) \to 0$. As we shall see in Sec. IV B, $w_{\text{eff}}(t)$ plays an important role in constraining the parameter space of these DDM ensembles.

B. Cosmological constraints

Given our time-dependent aggregate quantities $\Omega_{\text{tot}}(t)$, $\eta(t)$, and $w_{\text{eff}}(t)$, we now turn to the cosmological constraints that bound these functions. In this way, we shall ultimately be placing nontrivial constraints on the parameter space underlying these hadronic DDM ensembles.

In this connection, we again stress that our aim in this paper is not to perform a detailed analysis of the astrophysical and/or cosmological constraints on this parameter space. Such a detailed analysis would clearly be an important but extensive task which is beyond the scope of this paper. Moreover, such an analysis would require a

host of further assumptions concerning the particular nature of our ensemble, the specific decay modes of its constituents into SM states, and so forth. Rather, in this paper, our goal is to simply to obtain a rough initial sense of those regions of parameter space in which a DDM ensemble of dark "hadrons" might have at least the *potential* of phenomenological viability. Accordingly, in what follows, we shall put forth a set of requirements which directly constrain the fundamental quantities $\Omega_{tot}(t)$, $\eta(t)$, and $w_{eff}(t)$ we have defined above, but which do not require any further information concerning these hadronic ensembles beyond those properties already discussed. In some sense, then, these might be viewed as the immediate "zeroth-order" model-independent constraints that any DDM ensemble of this sort must satisfy.

Our first constraint is an obvious one: despite the presence of an infinite tower of dark-hadronic resonances, each with its own cosmological abundance and lifetime, we shall demand that

$$\Omega_{tot}(t_{now}) = \Omega_{CDM} \approx 0.26. \qquad (4.9)$$

This requirement is clearly predicated on the assumption that our dark-hadronic ensemble represents the totality of the dark sector; for other cases we would simply require that $\Omega_{tot}(t_{now}) \lesssim 0.26$. As we shall see, in either situation this is a severe and unavoidable constraint which ultimately "anchors" our entire construction in terms of actual numbers and mass scales.

Second, we may also consider the *time variation* of $\Omega_{tot}(t)$. The time variation of this total abundance is constrained by experimental probes which yield information about the dark-matter abundance during different cosmological epochs. For example, CMB data [24] provides information about the dark-matter abundance around the time of last scattering—i.e., at a redshift $z \approx 1100$, or equivalently a time of roughly $2.7 \times 10^{-5} t_{now}$. On the other hand, observational data on baryon acoustic oscillations [25] and the relationship between luminosity and redshift for Type Ia supernovae [26] provide information about $H(t)$ and the dark-energy abundance Ω_Λ at subsequent times, down to redshifts of around $z \approx 0.5$. Within the context of the ΛCDM cosmology, the agreement between these different measurements implies that the dark-matter abundance has not changed dramatically since the time of last scattering.

In order be consistent with this result, we shall therefore demand that the total abundance of our DDM ensemble not vary by more than 5% between an early "look-back" time t_{LB} and today:

$$\frac{\Omega(t) - \Omega(t_{now})}{\Omega(t_{now})} \leq 0.05 \quad \text{for all } t_{LB} \leq t \leq t_{now}. \quad (4.10)$$

In what follows, we shall choose a look-back time $t_{LB} = 10^{-6} t_{now}$, which lies comfortably before the recombination epoch.

In addition to these constraints on the time variation of the dark-matter abundance, there are further considerations which constrain the decays of the DDM-ensemble constituents more directly. These constraints depend on the decay properties of the dark-sector particles and are thus ultimately model-dependent. However, for those rather general cases in which the ensemble constituents can decay to final states involving visible-sector particles, one must ensure that these decay products not disrupt big-bang nucleosynthesis [27], not produce observable distortions in the CMB [28,29], not reionize the universe [30], and not violate current limits on the fluxes of photons or other cosmic-ray particles [31,32]. Indeed, even if the ensemble constituents decay exclusively into other, lighter dark-sector particles, such decays can nevertheless leave observable imprints on small-scale structure [33,34], alter the scale- and redshift dependence of the cosmological gravitational-lensing power spectrum [35], and affect the luminosity-redshift relation for Type Ia supernovae [36,37]. Since these effects all arise from the decays of ensemble constituents, nonobservation of these effects also leads to constraints on the time variation of Ω_{tot}.

Some of these latter constraints admittedly depend on model-dependent aspects of the decay kinematics of the dark-ensemble constituents. However the strongest and most general of these constraints effectively amount to limits on the variation of $\Omega_{tot}(t)$ within the recent past—i.e., for redshifts $0 \lesssim z \lesssim 3$. Therefore, in addition to our look-back-time constraint in Eq. (4.10), we shall also impose an additional constraint on our effective equation-of-state parameter:

$$w_{eff}(t_{now}) \leq 0.05. \qquad (4.11)$$

Through Eq. (4.7), this thus becomes a constraint on the present-day *time derivative* of $\Omega_{tot}(t)$. It is important to stress that this constraint is independent of that in Eq. (4.10): while Eq. (4.10) constrains accumulated changes in $\Omega_{tot}(t)$ over a relatively long interval, Eq. (4.11) constrains the time variation of $\Omega_{tot}(t)$ near the present time.

Other considerations will also guide our interest in certain regions of parameter space. For example, from a DDM-inspired standpoint, we are particularly interested in scenarios for which

$$\eta(t_{now}) \sim \mathcal{O}(1), \qquad (4.12)$$

i.e., scenarios in which the present-day value of η is significantly different from zero. This ensures that a sizable number of ensemble constituents continue to survive and contribute meaningfully to Ω_{tot} at the present time, with dark-matter decays occurring *throughout* the present epoch and not just in the distant past or future. Although Eq. (4.12) is not a strict requirement for phenomenological consistency, this condition guides the degree to which we

may regard our ensemble as being fully DDM-like, with a significant portion of the ensemble playing a nontrivial role in the phenomenology of the dark sector. For example, this condition rules out regions of parameter space in which $\tau_n \ll \tau_0$ for all $n \geq 1$, with $\tau_1 \ll t_{\rm LB}$. In such regions of parameter space, all excited dark-hadronic states have decayed prior to our look-back time, leaving us with a single dark-hadronic ground state in the present epoch. Such a scenario trivially satisfies all of our phenomenological constraints on the time variations of the total dark-sector abundance, but is effectively no different from that of a traditional, single-component dark sector. It is thus less interesting from a DDM perspective.

There are two further phenomenological constraints which will be useful for us to consider in the following. First, we shall demand that $\tau_0 \gg t_{\rm now}$. Although we do not necessarily require $\tau_0 \approx 10^9 t_{\rm now}$ as in traditional single-component dark sectors, we generally expect that τ_0 must exceed $t_{\rm now}$ by at least several orders of magnitude in order to satisfy look-back and $w_{\rm eff}$ constraints. This assumption will be discussed further in Sec. V. Likewise, although we have thus far assumed $M_0 \geq T_{\rm MRE}$ throughout our analysis, we actually must impose the somewhat stronger bound $M_0 \gtrsim \mathcal{O}(10^3) T_{\rm MRE} \approx \mathcal{O}$ (keV) in order to satisfy BBN and structure-formation constraints. This last requirement implicitly assumes that our lightest ensemble component carries the largest cosmological abundance (or at least a sizable fraction of the total cosmological abundance), but we shall see in Sec. V that this turns out to be true for the vast majority of phenomenologically interesting cases.

Finally, we shall also make certain simplifying assumptions. First, for concreteness, we shall restrict our attention to situations with $\xi = 3$. In other words, we shall assume that the dominant contributions to the decay lifetimes τ_n of our DDM constituents ϕ_n scale as $\tau_n \sim 1/M_n^3$ across the DDM ensemble. Decay widths of the form $\Gamma_n \sim M_n^3/\Lambda^2$ emerge naturally from operators such as $\phi_n F_{\mu\nu} F^{\mu\nu}/\Lambda$ where Λ parametrizes the energy scale associated with such couplings and where $F^{\mu\nu}$ denotes a field-strength tensor associated with either the visible-sector (SM) photon or a dark-radiation photon associated with an additional Abelian gauge group under which the ensemble constituents are not charged. The contributions from such operators will dominate the decays of our DDM constituents in scenarios in which our DDM ensemble is uncharged with respect to all SM symmetries, and in which intra-ensemble decays can be neglected. Likewise, we shall also make the simplifying assumption that $\kappa = 1$ in Eq. (2.2). This restricts us to the bare "minimal" case in which we do not ascribe nontrivial degrees of freedom to our dark-sector quarks, and thereby focus exclusively on the ensemble of states generated by our infinite tower of hadronic resonances. Finally, throughout our analysis, we shall continue to impose the self-consistency constraints listed in Eqs. (2.10) [or equivalently (2.11)], (2.12), (2.13), and (3.5).

Thus, going forward, the free parameters governing our dark-hadron DDM ensemble may be tallied as follows. First, there are the two parameters $\{B, C\}$ which govern the individual state degeneracies $\hat{g}_n$ according to Eq. (2.5). Second, there are the four parameters $\{r, s, M_0, \tau_0\}$ which govern the individual abundances $\Omega_n(t)$ in Eqs. (3.15) through (3.21). However, imposing Eq. (4.9) as an overall normalization condition allows us to remove M_0 as a free parameter. Thus, for the rest of this paper, we shall consider our DDM ensembles as functions of their locations within the five-dimensional parameter space corresponding to the variables $\{B, C, r, s, \tau_0\}$ where $B \geq 1$, $C^2 \geq 2\pi^2 (4B - 3)/3$, and $s \leq 1/C$.

V. RESULTS

In general, we seek to determine which values of our defining parameters $\{B, C, r, s, \tau_0\}$ lead to self-consistent and potentially viable dark sectors—i.e., sectors which satisfy our abundance, look-back, and $w_{\rm eff}$ constraints in Eqs. (4.9), (4.10), and (4.11) respectively, along with our $M_0 > \mathcal{O}$ (keV) constraint. For each such set, we also seek to determine the corresponding values of relevant mass scales such as the string scale M_s. We also seek to determine the extent to which the corresponding ensemble is truly DDM-like, with a relatively large number of component states playing a significant role in the phenomenology of the dark sector and contributing to $\Omega_{\rm tot}$ at the present time. In general, the larger the value of $\eta(t_{\rm now})$, the more DDM-like the corresponding ensemble.

At first glance, it might seem rather daunting to orient ourselves within the five-dimensional $\{B, C, r, s, \tau_0\}$ parameter space. However, there are really two separate parts to our analysis—one part which depends only on *relative* mass scales, and one part which makes explicit reference to *absolute* mass scales. It is clear from Eqs. (4.2) and (4.3) that once we know $\{B, C, r, s, \tau_0\}$, we can determine the function $\Omega_{\rm tot}^{\rm (R,NR)}(t)$ up to an overall multiplicative constant $\Omega_0^{\rm (R,NR)}(t_{\rm now})$. Setting $\Omega_{\rm tot}^{\rm (R,NR)}(t_{\rm now}) = \Omega_{\rm CDM} \approx 0.26$ therefore immediately determines a required numerical value of $\Omega_0^{\rm (R,NR)}(t_{\rm now})$. This also determines the corresponding values of $\eta(t_{\rm now})$ and $w_{\rm eff}(t_{\rm now})$. Up to this point, we have not yet anchored our results in terms of absolute mass scales. However, this can also easily be done: we simply set our required numerical value of $\Omega_0^{\rm (R,NR)}(t_{\rm now})$ to the expression in either Eq. (3.18) or Eq. (3.21). This then determines an absolute value for the mass scale M_0, whereupon we find that $M_s = r M_0$ and $T_c = (s/r) M_0$. Thus, in this way, we can extract the values for M_s and $\eta(t_{\rm now})$ corresponding to every point in the $\{B, C, r, s, \tau_0\}$ parameter space.

Certain observations can be made rather rapidly. For example, given Eq. (4.9), it immediately follows that $\Omega_0(t_{\rm now}) \lesssim 0.26$—a bound which can be saturated only when $\eta(t_{\rm now}) = 0$. More generally and more schematically,

we might write this constraint in the rough order-of-magnitude form

$$\Omega_0(t_{\text{now}}) \lesssim \mathcal{O}(0.1). \qquad (5.1)$$

However, let us now consider the expression in Eq. (3.21) for $\Omega_0(t)$ in the relativistic case. Since τ_0 must significantly exceed t_{now} by at least several orders of magnitude, as discussed in Sec. IV, we see that the exponential factor e^{-t/τ_0} is essentially 1. Likewise we recall that $M_0/T_{\text{MRE}} \geq \mathcal{O}(10^3)$, as also discussed in Sec. IV. Let us assume that this bound is saturated, so that $M_0/T_{\text{MRE}} = \mathcal{O}(10^3)$. We therefore find that Eq. (5.1) can be satisfied only if $g_c \sim 10^4$. This would in turn require a mass scale T_c which at the very minimum exceeds the TeV scale (thereby introducing a hierarchy between T_c and M_0 which is at least a factor of 10^6) and which actually must be so high that there are at least ten times as many effectively relativistic degrees of freedom below this scale than are known to exist below the TeV scale—a rather unlikely proposition resting entirely on currently unknown physics. Considering greater values of M_0/T_{MRE} only worsens this situation and requires even greater values of g_c. Therefore, although there might exist finely tuned slivers of parameter space in which one might manage to achieve a balancing between g_c and M_0/T_{MRE} sufficient to satisfy Eq. (5.1), we shall abandon any further consideration of the relativistic case in what follows.

This situation changes dramatically when we turn to the nonrelativistic case in Eq. (3.18). In this case, we continue to find that $e^{-t_{\text{now}}/\tau_0} \approx 1$. However, the presence of the factor $(r/s)^{3/2}e^{-r/s}$ allows us greater freedom in satisfying the constraint in Eq. (5.1). Indeed, the first thing we learn is that our system is going to be very sensitive to the ratio r/s—not surprising, given that this was already the radio that determined the extent to which our lightest mode was relativistic or nonrelativistic. However, we now see that r/s is also going to play a large role in governing the allowed values of the overall mass scales in our system, with greater (lesser) values of r/s generally corresponding to higher (lower) absolute mass scales for our ensemble.

We shall therefore proceed through our parameter space as outlined above, paying special attention to the values of r and s and in particular to the ratio r/s. Specifically, for each value of $\{B, C, r, s, \tau_0\}$, we shall determine whether our internal consistency constraints $B \geq 1$, $C^2 \geq 2\pi^2(4B - 3)/3$, and $s \leq 1/C$ are satisfied and whether the phenomenological consistency constraints in Eqs. (4.10) and (4.11) are satisfied. If so, we shall then determine the corresponding values of M_s and $\eta(t_{\text{now}})$, with the overall goal of understanding which regions of parameter space potentially lead to viable ensembles and which subregions correspond to ensembles which are particularly DDM-like.

Because of the somewhat natural and intuitive role played by the $D_\perp = 2$ scalar flux tube, as discussed in Sec. II, we shall adopt the values

$$B = 5/4, \qquad C = 2\pi/\sqrt{3} \approx 3.63 \qquad (5.2)$$

as "benchmark" values and begin our exploration within (r, s) space. Taking $\tau_0 = 10^9 t_{\text{now}}$, we find the results shown in Fig. 3.
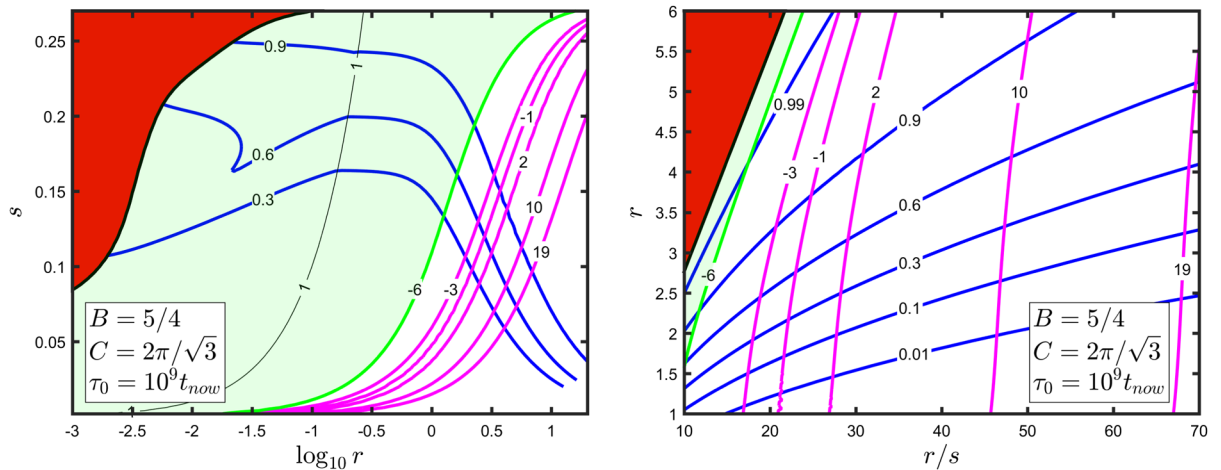

FIG. 3. A survey of physics in the (r, s) plane, with B, C, and τ_0 set to the "benchmark" values shown. Left panel: the thin black line labeled "1" indicates the contour with $r/s = 1$; this is thus the dividing line between the region in which the lightest state is relativistic (left of this line) versus nonrelativistic (right of this line). The blue curves indicate contours of $\eta(t_{\text{now}})$, while the magenta lines indicate contours of M_s and are labelled by the value of $\log_{10}(M_s/\text{GeV})$. The red region is excluded by look-back and w_{eff} constraints, while the pale green region is excluded by the constraint $M_0 \gtrsim \mathcal{O}$ (keV) which is saturated along the single green contour. Increasing (decreasing) the value of τ_0 does not affect the M_s or $\eta(t_{\text{now}})$ contours, and simply shifts the red exclusion region to the left (right). Right panel: same as left panel, but with features plotted relative to the variables r and r/s. The entire region shown in this panel corresponds to the nonrelativistic case.

Let us first concentrate on the left panel of Fig. 3. The red region indicates those values of (r, s) which are excluded by look-back and w_{eff} constraints, while the pale green region is excluded by the requirement that $M_0 \gtrsim \mathcal{O}$ (keV). The blue curves indicate contours of $\eta(t_{\text{now}})$ and the magenta curves indicate contours of M_s, labelled by values of $\log_{10}(M_s/\text{GeV})$. The single green curve indicates the contour with $M_0 = 1$ keV. The thin black curve indicates the contour with $r/s = 1$, and thus serves as the nominal dividing line between the regions in which the lowest ensemble state is relativistic (above and to the left) or nonrelativistic (below and to the right).

Several things are immediately apparent from this figure. First, we see that the portion of the parameter space corresponding to the relativistic case is excluded by our constraint on M_0. This is entirely in keeping with our conclusions already reached above. Nevertheless, we also see that beyond this region there exists an entire area of parameter space in which all of our constraints are satisfied. Moreover, within this region we see that M_s varies from the keV/MeV-range all the way to the Planck scale. Likewise, $\eta(t_{\text{now}})$ varies through all of its possible values. This is therefore not only an allowed region, but one which is likely to be exceedingly rich in phenomenology. Indeed, given the contours plotted in this figure, we see that the "sweet spot" within the (r, s) parameter space lies roughly within the range

$$\begin{cases} 1 \lesssim r \lesssim 6 \\ 0.05 \lesssim s \lesssim 0.18. \end{cases} \tag{5.3}$$

This is the region of (r, s) parameter space where the plotted blue and magenta contours intersect each other and form a "cross-hatched" region, as illustrated in the left panel of Fig. 3. This sweet spot is therefore the region that will be of maximum interest to us. Indeed, within this region, we observe from the left panel of Fig. 3 that $\eta(t_{\text{now}})$ increases if either r or s is increased, while M_s increases in the former case but decreases in the latter.

The right panel of Fig. 3 focuses on this sweet-spot region and shows the same M_s and η contours, only now plotted with respect to the variables r/s and s using a linear rather than logarithmic axis. The fact that the M_s contours are approximately vertical in this region indicates that M_s is dominantly determined by the ratio r/s, exactly as anticipated above, with increasing values of r/s corresponding to increasing values of M_s. Indeed, we see from the right panel of Fig. 3 that M_s increases extremely rapidly as a function of r/s, in keeping with the exponential dependence in Eq. (3.18). Likewise, increasing the value of r/s while holding r fixed tends to *decrease* the value of $\eta(t_{\text{now}})$. Thus, for fixed r, we find that M_s and $\eta(t_{\text{now}})$ tend to vary inversely with respect to each other as functions of r/s, with our ensembles becoming less DDM-like at higher mass scales and more DDM-like at lower mass scales.

Likewise, for fixed r/s, we find that increasing r tends to increase $\eta(t_{\text{now}})$, as already evident from the left panel of Fig. 3.

It is easy to understand these results physically. For fixed r, increasing r/s corresponds to decreasing s. This lowers the critical temperature T_c at which our initial cosmological abundances are established, which has the effect of decreasing the abundances of the heavier states relative to the lighter states. This therefore decreases the value of $\eta(t_{\text{now}})$. By contrast, holding r/s fixed and increasing r corresponds to increasing s as well. The increase in r renders all of the ensemble states more massive but provides a smaller proportional mass increase for the heavier states than for the lighter states. Thus the mass *ratios* between heavier and lighter states decreases, which tends to increase the value of $\eta(t_{\text{now}})$. Likewise, as discussed above, increasing s also tends to increase the value of $\eta(t_{\text{now}})$. These two effects then tend to reinforce each other, as evident in Fig. 3.

Having identified our sweet-spot region in (r, s) parameter space, we now investigate how these values of M_s and $\eta(t_{\text{now}})$ vary as our other parameters B, C, and τ_0 are varied. To do this, we study variations in these parameters relative to an (r, s) "benchmark"

$$r = 3.5, \qquad r/s = 30, \tag{5.4}$$

which we henceforth take as representative of our sweet-spot region in the (r, s) plane. In Fig. 4 we illustrate the effects of variations in B and C relative to this benchmark, plotting contours of M_s and $\eta(t_{\text{now}})$ in the (r, C) plane (upper left panel), the (s, C) plane (upper right panel), and the (B, C) plane (lower panel). Note that since we must always have $s \leq 1/C$, it is actually the normalized product $s \cdot C$ which captures the dependence on s in situations where C might also be varied. In the upper right panel we therefore plot our contours relative to $s \cdot C$ rather than s alone. Likewise, in the lower panel of Fig. 4 we have continued to indicate our allowed regions of B and C as in Fig. 1, where the dot continues to represent the $D_{\perp} = 2$ scalar-string benchmark values in Eq. (5.2).

Together, the three panels of Fig. 4 tell a consistent story. First, with r and s held fixed, we see from the upper left and lower panels of Fig. 4 that increasing C generally tends to increase $\eta(t_{\text{now}})$. This result makes sense: increasing C corresponds to increasing the *degeneracies* of the heavier states relative to the lighter states. However, with s held constant, each of these heavier states continues to accrue the same abundance as before. Thus increasing C increases the total abundance carried by the heavier states relative to that carried by the lighter states, thereby increasing $\eta(t_{\text{now}})$. Second, we see from the lower panel of Fig. 4 that while our values of M_s and $\eta(t_{\text{now}})$ are quite sensitive to C, they are far less sensitive to B. This too makes sense, since C governs the exponential rate of growth in the state
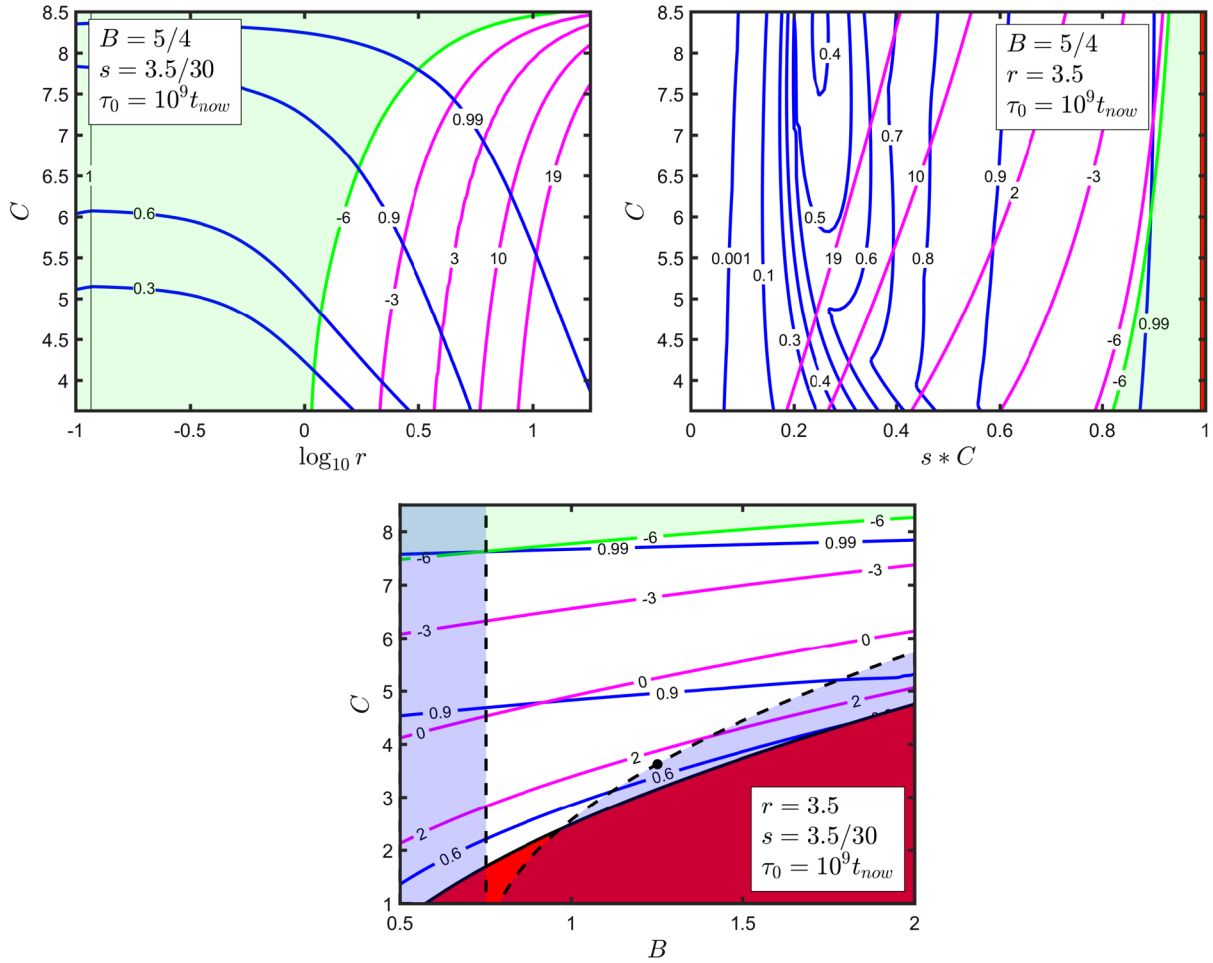
FIG. 4.   Contours of $\eta(t_{\mathrm{now}})$ (blue curves) and M_s (magenta curves), labelled as in Fig. 3 and plotted in three different planar "slices" through the (B, C, r, s) parameter space. The top two panels show these contours plotted in the (r, C) and (s, C) planes, respectively, while the bottom panel shows these contours plotted in the (B, C) plane. In all panels, colored shaded regions are excluded by either string consistency constraints (blue shaded regions), internal consistency constraints (red region in lower panel), or phenomenological look-back, w_{eff}, or $M_0 \gtrsim \mathcal{O}$ (keV) constraints (pale green regions as well as the red region along the right edge of the upper right panel). As in Fig. 3, the thin black vertical $r/s = 1$ contour (visible at the extreme left of the upper left panel) continues to represent the boundary between the regions in which the lightest state is either relativistic (left of the line) or nonrelativistic (right of the line).

degeneracies while B governs only the subleading polynomial behavior. Third, in each of the above two cases, we also note that increasing C while holding r or B fixed also corresponds to decreasing M_s. Thus, once again, we see that M_s and $\eta(t_{\mathrm{now}})$ tend to vary inversely with each other, giving rise to more DDM-like ensembles at lower energy scales and more traditional ensembles at higher energy scales.

Finally, we see from the upper right panel of Fig. 4 that our values of $\eta(t_{\mathrm{now}})$ are largely *insensitive* to variations in C as long as $s \cdot C$ is held fixed. However, this too is easy to understand. Increasing C while holding $s \cdot C$ fixed corresponds to decreasing s as we increase C. Increasing C induces an exponential increase in the degeneracy of each massive state, while decreasing s decreases the critical temperature T_c, thereby inducing a corresponding exponential decrease in the abundance associated with each such

state. Thus, to first approximation, these two effects tend to mitigate each other: they produce more states, but also cause each state to carry a correspondingly smaller abundance.

Thus far we have not discussed the effects of varying our remaining free parameter τ_0. Varying τ_0 does not affect the degeneracies of states or their cosmological abundances. Indeed, variations in τ_0 affect only the *lifetimes* of these states. In principle, this has the potential to affect the values of quantities such as $\eta(t_{\mathrm{now}})$ since the determination of $\eta(t_{\mathrm{now}})$ requires totalling the abundances of only those states which have not yet decayed at the present time. However, under the assumption that $\tau_0 \gg t_{\mathrm{now}}$ (or under the equivalent assumption that our scenario already satisfies the look-back and w_{eff} constraints), we know that $\Omega_{\mathrm{tot}}(t_{\mathrm{now}})$ is not changing rapidly at the present time. In other words, the total abundances of those states which are decaying at the
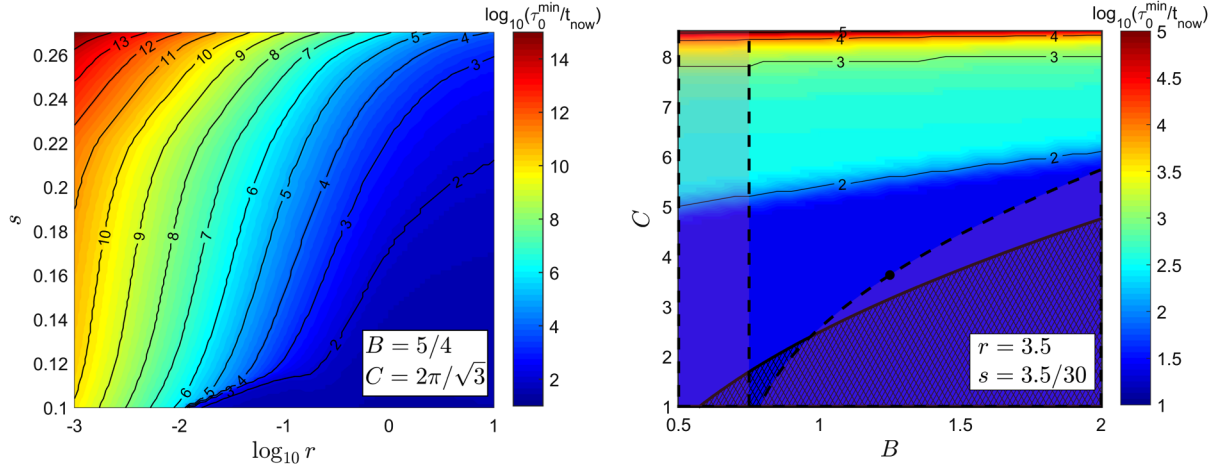
FIG. 5. Contours of the minimum value of $\tau_0^{\min}$ consistent with the look-back and w_{eff} constraints discussed in the text, plotted in the (r, s) plane (left panel) and in the (B, C) plane (right panel).

present time is relatively small. In such cases, the M_s and $\eta(t_{\text{now}})$ contours are therefore largely insensitive to τ_0. Indeed, in Fig. 3, the sole effect of varying τ_0 is therefore merely to "slide" the red exclusion regions in Fig. 3 horizontally relative to the rest of the plot: these exclusion regions move to the right (and therefore become more threatening to our sweet-spot region) if τ_0/t_{now} is decreased, and move to the left (and therefore become even less of a concern) if τ_0/t_{now} is increased.

While this is entirely as expected, the natural question then arises: for any values of $\{B, C, r, s\}$, what is the minimum value of τ_0 that can be tolerated before violating our look-back and w_{eff} constraints? Contours indicating the resulting minimum values $\tau_0^{\min}$ are plotted in Fig. 5 in both the (r, s) and (B, C) planes, taking our "benchmark" values in Eqs. (5.4) and (5.2) respectively. In general, we see from Fig. 5 that a wide variety of values of $\tau_0^{\min}$ are possible, depending on our specific location in parameter space, with larger values of $\tau_0^{\min}$ corresponding to very small values of r or relatively large values of s or C. However, for our sweet-spot benchmark values in Eqs. (5.2) and (5.4), we see from Fig. 5 that $\tau_0^{\min}$ can be as small as approximately $10^2 t_{\text{now}}$.

This, too, is not entirely a surprise. After all, a bound on the lifetime of the longest-lived DDM constituent on the order $\tau_0/t_{\text{now}} \sim \mathcal{O}(100)$ is roughly on the same order as the most conservative bounds on the lifetime τ_χ of a traditional single-component dark-matter candidate which decays into other purely dark-sector states. Indeed, model-independent bounds on decaying dark matter in traditional single-component models in which the dark-matter particle carries essentially all of the observed dark-matter abundance and decays into dark radiation have been derived by a number of groups (see, e.g., Refs. [38–42]). Depending on the assumptions inherent in the various analyses and on the breadth of cosmological data incorporated, such studies place a bound on the lifetime of such a dark-matter

candidate on the order of $\tau_\chi/t_{\text{now}} \gtrsim \mathcal{O}(10\text{–}100)$. Thus, a bound on τ_0 in this range is *a priori* reasonable—especially since our analysis in Fig. 5 determines the value of $\tau_0^{\min}$ based only on cosmological look-back and w_{eff} constraints. Of course, if the ensemble constituents decay into *visible*-sector particles with a non-negligible branching fraction, the constraints on τ_0 are expected to increase significantly. Indeed, the most stringent bounds on a single dark-matter particle χ which decays primarily into visible-sector radiation require that this particle be hyperstable, with $\tau_\chi \sim 10^9 t_{\text{now}}$.

Despite the possibilities for lowering τ_0 afforded by the results in Fig. 5, we shall continue to retain our benchmark value $\tau_0 = 10^9 t_{\text{now}}$. We do this in order to be consistent with the most conservative decay scenarios possible. Although this value for τ_0 is quite large, we emphasize that this is only the lifetime of the lightest ensemble constituent, and that a significant fraction of the ensemble constituents will generally have lifetimes much less than τ_0. Moreover, even in cases for which the majority of the ensemble is long-lived, DDM ensembles can nevertheless yield striking astrophysical signatures [6–8] which differ from those of traditional dark-matter candidates. Thus, even with such values of τ_0, the phenomenology of the resulting ensemble can differ significantly from that of traditional dark-matter candidates.

Having explored the relevant $\{B, C, r, s, \tau_0\}$ parameter space of our ensemble and identified our sweet-spot region, we now examine the characteristics of the corresponding ensembles in more detail. In particular, we seek to understand what these ensembles look like, and how their overall structure evolves with time. As discussed in Sec. IV A, the most relevant aggregate properties of any dark-sector ensemble are its total cosmological abundance $\Omega_{\text{tot}}(t)$, its effective equation-of-state parameter $w_{\text{eff}}(t)$, and its tower fraction $\eta(t)$, each of which is generally time-dependent. We therefore begin by examining how each of these

quantities evolves with time for ensembles in and near our sweet spot.

This information is shown in Fig. 6. In this figure, we consider a "benchmark" ensemble with $B = 5/4$, $C = 2\pi/\sqrt{3}$, $r = 3.5$, $s = 3.5/30$, and $\tau_0 = 10^9 t_{\text{now}}$, as well as nearby ensembles in which τ_0 is varied (top row), r is varied (second row), s is varied (third row), C is varied (fourth row), and B is varied (fifth row). In each case, we plot the corresponding total cosmological abundance Ω_{tot} (left column), equation-of-state parameter w_{eff} (middle column), and tower fraction η (right column) as functions of time. Note that in each case the overall abundance is normalized through an appropriate choice of M_s such that $\Omega(t_{\text{now}}) = \Omega_{\text{CDM}} \approx 0.26$, as required.

In each panel of Fig. 6 (except for those along the bottom row), the blue curve corresponds to our "benchmark" point. We therefore begin by focussing on these benchmark curves. The curve for $\Omega_{\text{tot}}(t)$ appears nearly constant at $\Omega_{\text{CDM}} \approx 0.26$ for all of the cosmological history plotted (which we assume to have been matter-dominated), including the present time t_{now}. Indeed, this behavior continues all the way into the future until $t \approx 10^9 t_{\text{now}}$, at which point $\Omega_{\text{tot}}(t)$ begins to decline gently to $\Omega_{\text{tot}} = 0$. This behavior is matched by $w_{\text{eff}}(t)$, which remains near zero for most its cosmological evolution before gently rising to $w_{\text{eff}} > 0$ at $t \approx 10^9 t_{\text{now}}$. This makes sense, since Eq. (4.7) tells us that $w_{\text{eff}}(t)$ is proportional to the time derivative of $\Omega_{\text{tot}}(t)$. Finally, we see that $\eta(t)$ remains more or less fixed at approximately $\eta \approx 0.72$ during most of its cosmological history before smoothly dropping to $\eta = 0$.

This behavior is easy to understand. If this has been a traditional ensemble with a single dark-matter component whose decay we could model as essentially instantaneous (just as we are assuming for the individual components of our dark-matter ensembles), our curve for $\Omega_{\text{tot}}(t)$ would have been fixed precisely at its present value $\Omega_{\text{CDM}} \approx 0.26$ over the entire range shown until suddenly dropping (essentially discontinuously) to $\Omega_{\text{tot}} = 0$ when the single dark-matter particle decays at $t \approx 10^9 t_{\text{now}}$. Likewise, $w_{\text{eff}}(t)$ would have been strictly fixed at $w_{\text{eff}} = 0$ during the cosmological evolution, while $\eta(t)$ would have been fixed at zero all along. However, this is not a traditional dark-matter setup: this is a DDM ensemble in which the present-day cosmological abundance $\Omega_{\text{tot}}(t_{\text{now}}) \approx 0.26$ is spread across a relatively large number of individual components with different masses and different lifetimes. It is thus the continued, ordered, sequential decays of these different components which produce the softer, gentler drop in $\Omega_{\text{tot}}(t)$ as t approaches $t \approx 10^9 t_{\text{now}}$. In fact, $\Omega_{\text{tot}}(t)$ is actually falling slightly *throughout* the cosmological evolution shown; this behavior is not visible in Fig. 6 only because at early times prior to $t \approx 10^9 t_{\text{now}}$ the states which are decaying are extremely heavy and thus carry extremely small abundances. By contrast, at late times approaching $t \approx 10^9 t_{\text{now}}$, the states which are decaying are relatively

low-lying and carry more significant abundances. This is also evident in our curve for $\eta(t)$: for most of the cosmological history, the value $\eta \approx 0.72$ tells us that only approximately 28% of the total dark-sector cosmological abundance is carried by the dominant (lightest) state in the ensemble, even at early times, while the remaining 72% of the abundance is carried by the more massive states— particularly those which, though more massive, are nevertheless relatively low-lying. As a result of the sequential decays of such states, $\eta(t)$—like $\Omega_{\text{tot}}(t)$—is also actually falling slightly *throughout* the cosmological evolution shown. It is only due to the decays of the relatively low-lying states near $t \approx 10^9 t_{\text{now}}$ that $\eta(t)$ ultimately falls gently but noticeably to zero.

At first glance, it may seem surprising that all three of our primary quantities Ω_{tot}, w_{eff}, and η are nearly constant at $t \approx t_{\text{now}}$. However, this is ultimately the direct consequence of our benchmark choice $\tau_0 = 10^9 t_{\text{now}}$: with this choice, those states within the ensemble which are decaying today are all extremely massive and thus carry very little abundance. The DDM nature of such an ensemble is nevertheless clear from its η-value, which is as high as 0.72 even at the present time. In this connection, we again emphasize that taking $\tau_0 = 10^9 t_{\text{now}}$ was merely a conservative choice which is not by itself intrinsic to the DDM framework; indeed we learned from Fig. 5 that we could easily have chosen τ_0 as small as $\tau_0 \approx 10^2 t_{\text{now}}$ without running afoul of our look-back and w_{eff} constraints. Indeed, without further details concerning the precise nature of these ensembles (including, most critically, the ultimate decay products of their constituents), such small values for τ_0 would have been equally viable.

This observation is illustrated along the top row of Fig. 6, where we show the evolution of our blue "benchmark" curves as we vary τ_0 between our conservative value $\tau_0 \approx 10^9 t_{\text{now}}$ and the more extreme value $\tau_0 \approx 10^2 t_{\text{now}}$. In general, changing τ_0 does not affect the internal structure of the ensemble—it merely affects the lifetimes of the individual ensemble constituents, rescaling them all up or down together. Since it is these lifetimes which produce the nontrivial time dependence for Ω_{tot}, w_{eff}, and η, we expect that changing τ_0 should preserve the general shapes of these curves and merely translate these curves along the time axis. This behavior is verified in the panels along the top row of Fig. 6. Indeed, we can even see from these panels why $\tau_0 \approx 10^2 t_{\text{now}}$ is the minimum value of τ_0 that may be chosen for our benchmark point: choosing τ_0 any smaller would shift our curves even further towards earlier times, whereupon $\Omega_{\text{tot}}(t)$ would begin to experience significant variations within the interval $10^{-6} t_{\text{now}} \lesssim t \lesssim t_{\text{now}}$ and $w_{\text{eff}}(t_{\text{now}})$ would begin to deviate significantly from zero. Such behavior would then violate our look-back and w_{eff} constraints, respectively.

Let us now turn to the behavior of our Ω_{tot}, w_{eff}, and η curves as we vary r, as shown in the panels along the
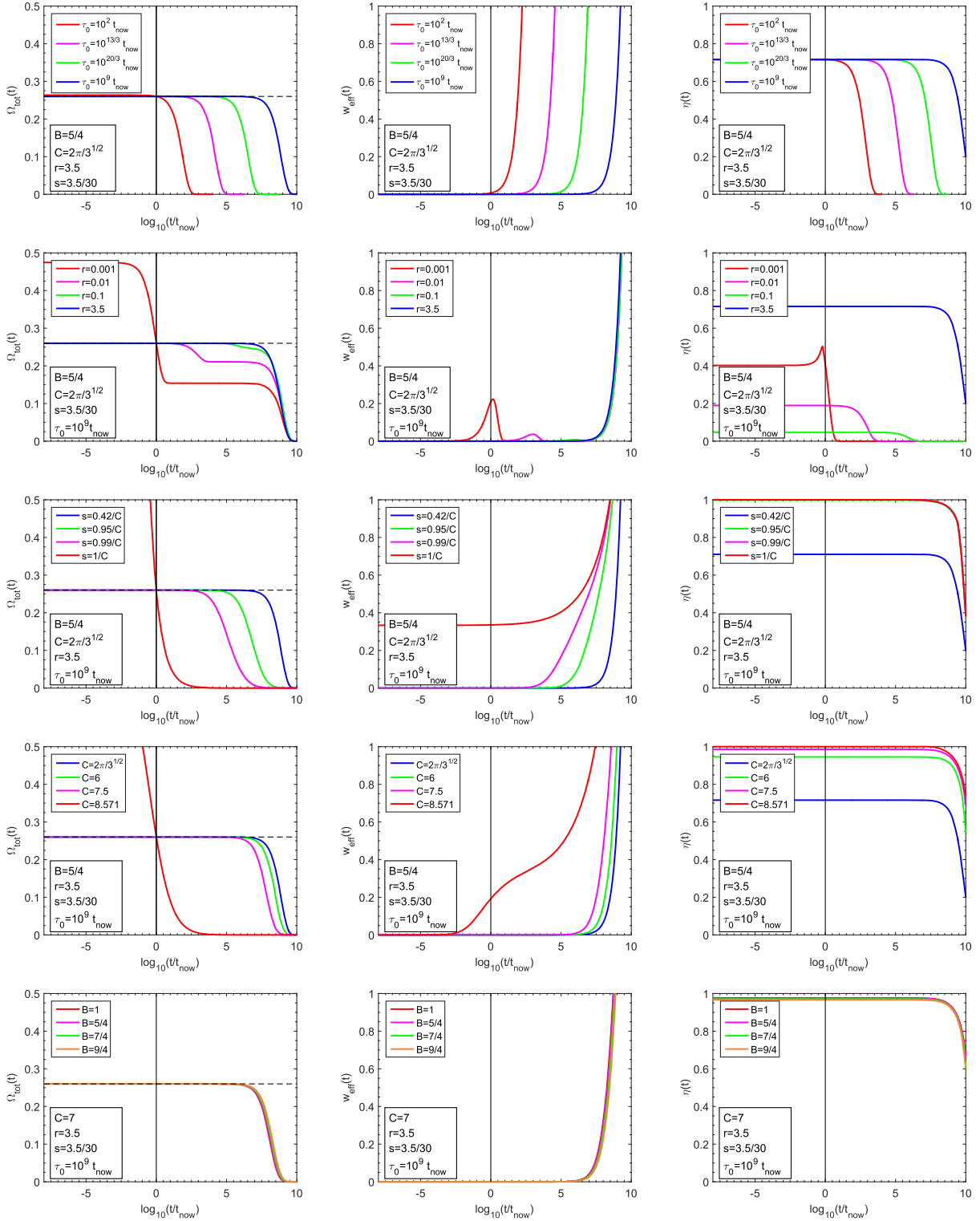
FIG. 6. Total cosmological abundances $\Omega_{\rm tot}$ (left column), equation-of-state parameters $w_{\rm eff}$ (middle column), and tower fractions η (right column) for our DDM ensembles, plotted as functions of time when all input variables are held fixed at their "benchmark" values except for τ_0 (top row), r (second row), s (third row), C (fourth row), and B (bottom row). In all panels the blue curve corresponds to our "benchmark" point with $B = 5/4$, $C = 2\pi/\sqrt{3}$, $r = 3.5$, $s = 3.5/30$, and $\tau_0 = 10^9 t_{\rm now}$, while the curves of other colors indicate departures away from this point. For reasons discussed in the text, the bottom row illustrates variations in B along a line that does not include the benchmark point. Note that, as expected, some variations away from the benchmark point violate our look-back, $w_{\rm eff}$, or M_0 constraints. However, our internal self-consistency constraints are always satisfied, with $\Omega_{\rm tot}(t_{\rm now}) = \Omega_{\rm CDM} \approx 0.26$ in all cases.

second row of Fig. 6. Two observations underlie the behavior shown. First, we note that changing r changes the lifetimes of the states at each mass level according to Eq. (3.14), with $\tau_n/\tau_0 \to 0$ as $r \to 0$. This result is simple to understand: as $r \to 0$, the $n = 0$ states become hierarchically lighter than the $n \geq 0$ states and thus the $n > 0$ states have hierarchically shorter lifetimes. Second, we note that changing r also changes the relative abundances which are generated at t_c according to

$$\frac{\Omega_n(t_c)}{\Omega_0(t_c)} = \frac{(n + r^2)^{5/4}}{r^{5/2}} \exp\left(-\frac{\sqrt{n + r^2} - r}{s}\right). \quad (5.5)$$

This quantity is nonmonotonic as a function of r, first dropping as r is reduced from large values and ultimately hitting a minimum before increasing again and diverging as $r \to 0$. Indeed, for $n = 1$ and s set to its benchmark value $s = 3.5/30 \approx 0.117$, this minimum occurs at $r \approx 0.4$.

These two effects are responsible for the behaviors shown in the second row of Fig. 6. As r decreases from its benchmark value with τ_0 held fixed, the excited states with $n > 0$ start decaying earlier and earlier. Rescaling our overall abundances in order to keep $\Omega_{\text{tot}}(t_{\text{now}}) = \Omega_{\text{CDM}}$ produces the effects shown in the left panel. Indeed, we see from this panel that the case with $r = 0.001$ actually violates our look-back and w_{eff} constraints, as already evident from Fig. 3. Even the $\Omega_{\text{tot}}(t)$ curve with $r = 0.01$ is tightly constrained: shifting τ_0 towards any smaller values below $10^9 t_{\text{now}}$ (i.e., shifting this curve further towards the left) also leads to violations of our look-back and w_{eff} constraints, as already anticipated in the left panel of Fig. 5. Likewise, as a result of the observations below Eq. (5.5), the relative sizes of the abundances Ω_n associated with the excited $n > 0$ states relative to the abundance Ω_0 associated with the $n = 0$ ground state vary nonmonotonically with r, shrinking as r drops from 3.5 to approximately 0.4, and then growing again as r drops still further. This then explains the nonmonotonic behavior for $\eta(t)$ as a function of r, as shown in the right panel.

By contrast, the effects of varying s and C are shown along the third and fourth rows of Fig. 6, respectively. While the quantity s governs the exponential rate at which the Boltzmann suppression of the abundances of the ensemble constituents *decreases* with n, the quantity C governs the exponential rate at which the degeneracy of states for the ensemble *grows* with n. As a result, the effects of decreasing s or increasing C are largely similar to each other as far as $\Omega_{\text{tot}}(t)$ is concerned, as evident in Fig. 6: both tend to increase the primordial aggregate abundances $\hat{\Omega}_n$ of the heavier states in the ensemble. This effect causes $\Omega_{\text{tot}}(t)$ to begin to decline earlier and earlier as these heavier states are the first to decay. By contrast, it is important to note that increasing C and decreasing s nevertheless have *opposite* effects on the value of $\eta(t_{\text{now}})$: the former increases $\eta(t_{\text{now}})$, as anticipated in Fig. 4, while the latter decreases $\eta(t_{\text{now}})$, as

anticipated in Fig. 3. This difference occurs because increasing C merely increases the state degeneracies $\hat{g}_n$ of the heavy states, thereby injecting more abundance into the heavy states relative to the light states, while decreasing s has the effect of increasing the abundances of *all* of our states, including the abundance of the dominant abundance carrier at $n = 0$. This causes the total abundance of the ensemble to grow more rapidly than the abundances of the excited $n > 0$ states alone, thereby decreasing $\eta(t_{\text{now}})$.

One important feature to note from these plots is the appearance of a Hagedorn instability as $s \to 1/C$ (or equivalently as $C \to 1/s$). In these limiting cases, the total energy density Ω_{tot} injected into the system through our confining phase transition at $t = t_c$ diverges, violating the constraint in Eq. (3.4). Such cases therefore violate our look-back and w_{eff} constraints, as evident in Fig. 6. Indeed, the Hagedorn instability is a critical feature of theories with exponentially growing degeneracies of states [12].

Finally, we turn to the fifth and final row of Fig. 6. Note that in order to remain within the self-consistency bound in Eq. (2.13), it is not possible to increase B above our benchmark value 5/4 when $C = 2\pi/\sqrt{3}$. For this reason, we have chosen to hold C fixed at a greater value, specifically $C = 7$, when exploring the effects of varying B. Unfortunately, we see that variations in B are barely distinguishable in these plots, even when B is varied all the way from $B = 1$ (corresponding to $D_\perp = 1$) to $B = 9/4$ (corresponding to $D_\perp = 6$). This tells us that the sorts of abundance-based or equation-of-state-based analyses we are doing here are relatively insensitive to the number of uncompactified transverse spacetime directions into which our dark-sector flux tube can vibrate, as long as C (related to the total central charge of the degrees of freedom on the flux-tube worldsheet) is held fixed. Of course, in a realistic setting, there are likely to be many other more specific probes of $D_\perp$, including probes that are based on specific properties of the dark-sector dynamics. Our result here merely indicates that studies based on cosmological abundances alone are not likely to be the most useful in this regard.

We have seen in Fig. 6 how the total abundances Ω_{tot} of our DDM ensembles vary as a function of time. However, it is also interesting to understand how the *individual* aggregate abundances $\hat{\Omega}_n(t)$ at each mass level n contribute to this behavior. The result is shown in Fig. 7 for our benchmark DDM model. As we see from Fig. 7, there are many mass levels n whose states contribute to $\Omega_{\text{tot}}(t_{\text{now}})$: states with smaller values of n carry larger abundances and have longer lifetimes, persisting into later times before decaying, while those with larger values of n carry smaller abundances and have shorter lifetimes, decaying earlier. Indeed, this balancing between lifetimes and abundances is a fundamental hallmark of the DDM framework. Although the sum of these abundances at $t = t_{\text{now}}$ is fixed at $\Omega_{\text{tot}}(t_{\text{now}}) = \Omega_{\text{CDM}} \approx 0.26$, we see that even
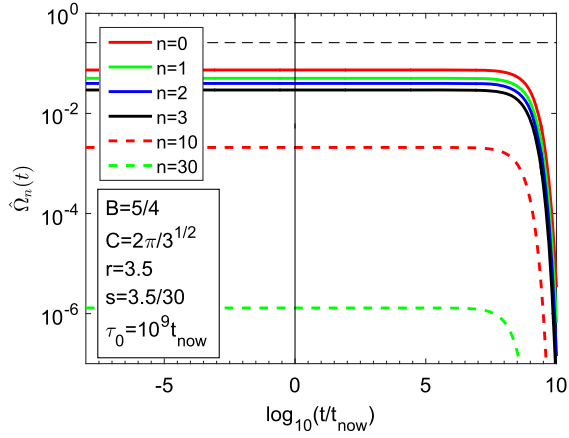
FIG. 7. The level-by-level aggregate cosmological abundances $\hat{\Omega}_n \equiv g_n\Omega_n$ of our benchmark DDM model, plotted as functions of time for a series of low-lying mass levels n. We see that the lightest states decay later and carry the largest cosmological abundances, while the heavier states decay earlier and carry smaller cosmological abundances—a key feature of the DDM framework. As required, the sum of all abundance contributions at $t = t_{\text{now}}$ is $\Omega_{\text{tot}}(t_{\text{now}}) = \Omega_{\text{CDM}} \approx 0.26$.

states with relatively large values of n have lifetimes τ_n exceeding t_{now} and thus contribute nontrivially to $\Omega_{\text{tot}}(t_{\text{now}})$. Indeed, for our benchmark model, we find that there are no fewer than seven distinct mass levels contributing more than 0.01 to $\Omega_{\text{tot}}(t_{\text{now}})$ and no fewer than ten distinct mass levels contributing more than 1% of $\Omega_{\text{tot}}(t_{\text{now}})$.

It is also interesting to examine how these results vary as a function of the ratio r/s which, as we have seen, governs the overall mass scales associated with these DDM ensembles. The results are shown in Fig. 8, where we plot the aggregate fractions $\hat{\Omega}_n(t_{\text{now}})/\Omega_{\text{tot}}(t_{\text{now}})$ for a variety of different mass levels n as a function of r/s. As evident in Fig. 8, the lightest state carries a larger and larger fraction of the total abundance as r/s increases, resulting in scenarios which have smaller values of η and which are therefore less DDM-like. By contrast, the lightest state carries a smaller proportional fraction of the total abundance as r/s decreases, and in fact may not even be the dominant state for sufficiently small r/s. Indeed, for $r/s = 15$, we find that all states carry relatively small abundances, and it is actually the states at the $n = 23$ mass level which collectively carry the largest individual abundance at the present time. Such scenarios are therefore extremely DDM-like.

Putting all the pieces together, we can summarize our results as in Figs. 9 and 10. Figure 9 consists of a sequence of dark-matter pie charts showing the relative contributions to $\Omega_{\text{tot}}(t_{\text{now}}) = \Omega_{\text{CDM}} \approx 0.26$ from the lowest-lying states for $r = 3.5$ (top row) and $r = 4$ (bottom row), with $r/s = \{25, 30, 50, 65\}$ across each row. Within each pie, we illustrate the corresponding collective abundances $\hat{\Omega}_n(t_{\text{now}})$ as separate slices, one for each value of n, while the numbers listed within each slice indicate the number of individual states $\hat{g}_n$ contributing at that mass level. For each pie chart we have also shown the corresponding values of M_0, T_c, and M_s. For these calculations we have used the input values $T_{\text{MRE}} = 0.7756$ eV, $g_{\text{MRE}} = 3.36$, and $g_c = \{10.75, 61.75, 106.75, 106.75\}$, respectively, for $r/s = \{25, 30, 50, 65\}$. We have also assumed our standard benchmark values $B = 5/4$, $C = 2\pi/\sqrt{3}$, and $\tau_0 = 10^9 t_{\text{now}}$.

Let us begin by focusing on the "benchmark" pie chart within Fig. 9 corresponding to $r = 3.5$ and $r/s = 30$.
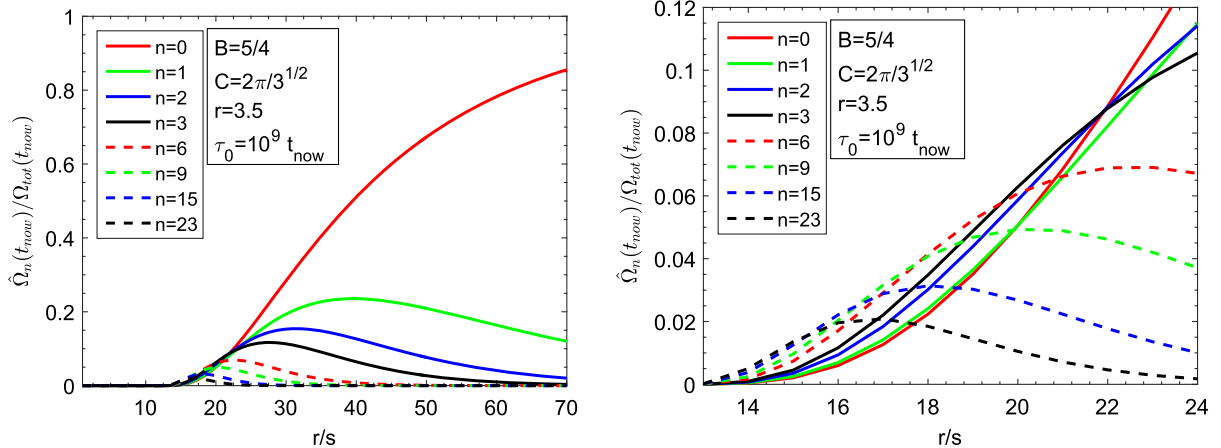

FIG. 8. Left: present-time aggregate abundance fractions $\hat{\Omega}_n(t_{\text{now}})/\Omega_{\text{tot}}(t_{\text{now}})$, plotted as functions of r/s. As r/s increases, the $n = 0$ state carries an increasingly large fraction of the total abundance, resulting in scenarios which have smaller values of η and which are therefore less DDM-like. By contrast, for smaller r/s, we see that the lightest state carries a smaller proportional fraction of the total abundance and in fact may not even be the dominant state for sufficiently small r/s. Right: closeup of the left panel, illustrating how the level n of the states carrying the largest collective abundance $\Omega_n(t_{\text{now}})$ shifts as a function of r/s. For example, for $r/s = 15$, all states carry relatively small abundances and it is actually the $n = 23$ states which collectively carry the largest collective abundance at the present time. Such scenarios are therefore extremely DDM-like.
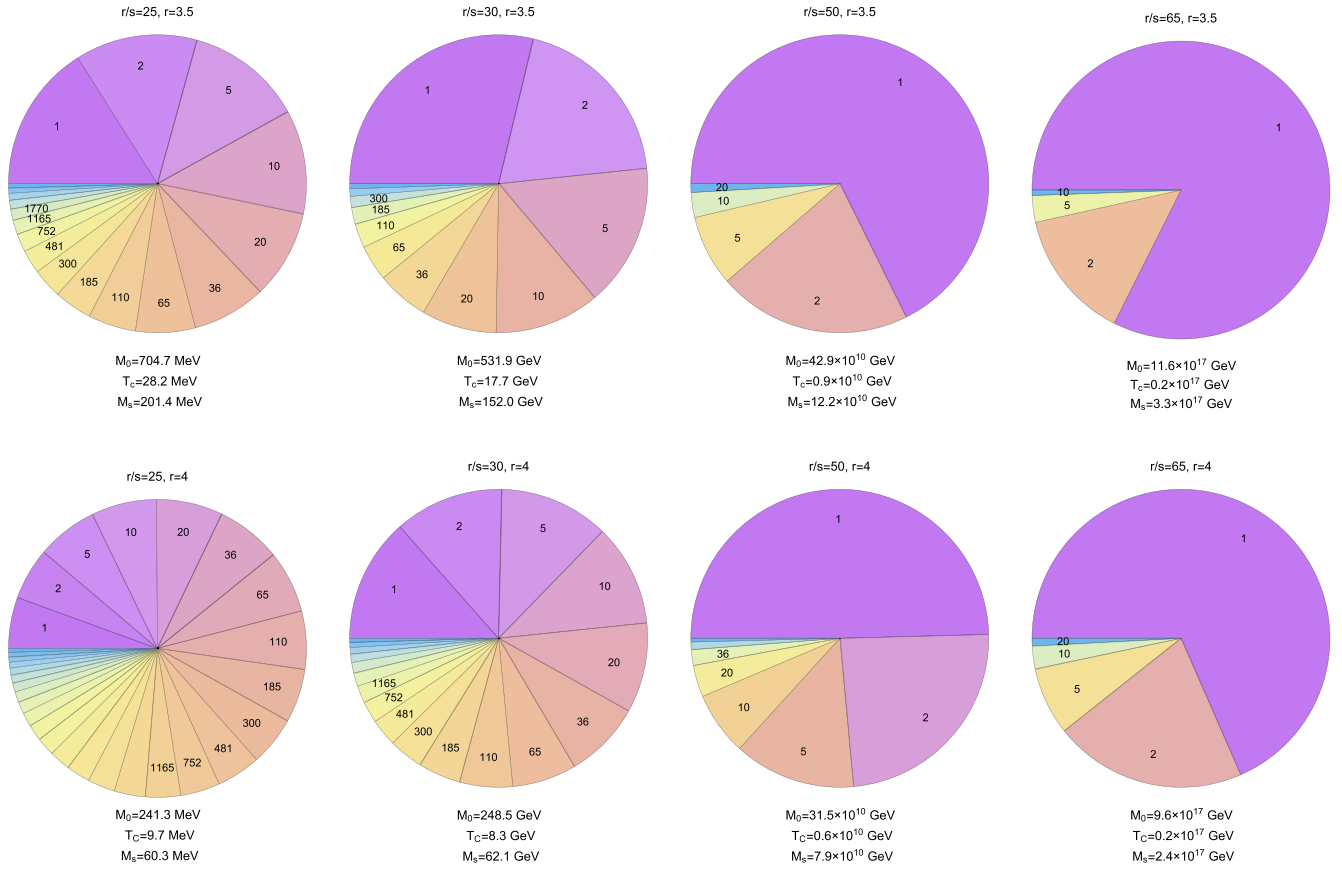
FIG. 9. Dark-matter pie charts showing the relative contributions to $\Omega_{\text{tot}}(t_{\text{now}}) = \Omega_{\text{CDM}} \approx 0.26$ from the lowest-lying states for $r = 3.5$ (top row) and $r = 4$ (bottom row), with $r/s = \{25, 30, 50, 65\}$ across each row and with $B = 5/4$ and $C = 2\pi/\sqrt{3}$ held fixed. In the majority of cases (but not all cases), the largest pie slice corresponds to the abundance contribution from the $n = 0$ mass level, and the successively smaller pie slices (progressing in a clockwise fashion within the pie chart) correspond to the aggregate abundance contributions from successively higher mass levels. Within each pie slice we have also indicated the degeneracy $\hat{g}_n$ of individual states whose cosmological abundances comprise the contribution from that slice. Note that in each case, the pie shown only corresponds to the dark-matter slice $\Omega_{\text{CDM}} \approx 0.26$ of the bigger "cosmic pie" which also includes contributions from dark energy and visible matter.

For this pie chart, we see that the largest pie slice corresponds to the abundance contribution from the $n = 0$ mass level, while the successively smaller pie slices progressing in a clockwise fashion within the pie chart correspond to the abundance contributions from successively higher mass levels. For this pie chart, we find that $M_0 \approx 532$ GeV, $T_c \approx 18$ GeV, and $M_s \approx 152$ GeV. Note that this value for M_s is in agreement with the M_s contours shown in Fig. 3. We also see geometrically from this pie chart that $\eta \approx 0.72$, in agreement with the results shown in Figs. 3, 4, and 6.

Given this, we can now investigate how this benchmark pie chart deforms as a function of r/s and r. Results are illustrated in the other pie charts shown in Fig. 9. We see in general that increasing r from 3.5 to 4.0 (i.e., passing from the top row of pie charts in Fig. 9 to the bottom row) has the net effect of shifting cosmological abundance away from the ground state, thereby increasing η and generally making each pie slice smaller while simultaneously lowering the corresponding mass scales. This is in complete accord with

the results shown in Fig. 3. Likewise, decreasing or increasing r/s (i.e., moving left or right along either row) has the effect of increasing or decreasing η while decreasing or increasing our corresponding mass scales. Indeed, we see that the variable r/s allows us to interpolate between two extremes: traditional ensembles with high mass scales at large r/s versus DDM-like ensembles with smaller mass scales at small r/s. We further observe that for sufficiently small r/s, the largest pie slice is no longer the $n = 0$ slice (labelled "1" in each pie chart)—as r/s decreases, this honor gradually shifts towards the pie slices corresponding to higher mass levels. This is in accordance with the results in Fig. 8.

Figure 10 is similar to the top row of Fig. 9, except that we have now increased our values of C and B to $\sqrt{2}\pi$ and $B = 3/2$, respectively. These new values maintain $c_{\text{int}} = 0$ and correspond to the $D_\perp = 3$ scalar string. These changes in C and B increase the degeneracies $\hat{g}_n$ of states at each mass level, with the new values indicated within the corresponding pie slices. Although the cosmological
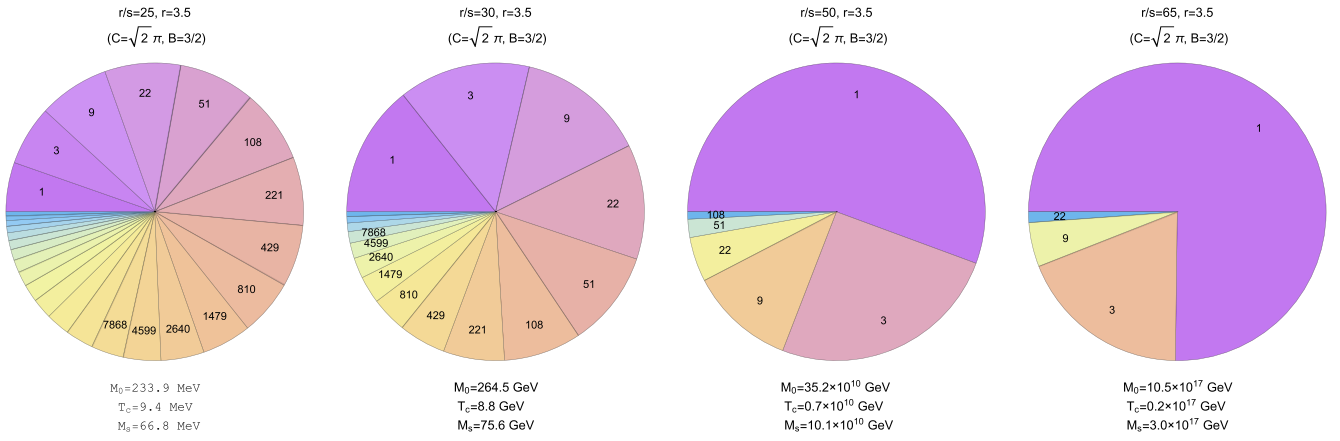
FIG. 10.   Same as the top row of Fig. 9 except that we have now taken $C = \sqrt{2}\pi$ and $B = 3/2$, corresponding to the $D_\perp = 3$ scalar string. These changes in C and B change the degeneracies $\hat{g}_n$ of states at each mass level, as indicated within the corresponding pie slices, and result in ensembles which are even more DDM-like and which have correspondingly smaller mass scales than those along the top row of Fig. 9.

abundances per state are not affected by the changes in C and B, these increased degeneracies result in ensembles which are even more DDM-like and which have correspondingly smaller mass scales than those along the top row of Fig. 9. These results are consistent with those shown in Fig. 4.

We see, then, that a tremendous variety of DDM ensembles exist which have the two fundamental features outlined in the Introduction—Regge trajectories and exponentially rising degeneracies of states. These ensembles are consistent with our look-back and w_{eff} constraints, and thus satisfy the zeroth-order constraints that may be imposed on such ensembles on the basis of their total energy densities and equations of state alone. We also observe an important feature, an inverse correlation between the tower fraction η (which governs the extent to which our ensemble is truly DDM-like) and the magnitude of its underlying mass scales. Indeed, we have seen that while traditional ensembles typically have high corresponding mass scales, our ensembles become increasingly DDM-like for lower mass scales—all while remaining consistent with our look-back and w_{eff} constraints. These observations will likely be an important guide and ingredient in any future attempts to build realistic dark-matter models of this type.

VI. CONCLUSIONS

In this paper, we have investigated the properties of a hitherto-unexplored class of DDM ensembles whose constituents are the composite states which emerge in the confining phase of a strongly-coupled dark sector. In ensembles of this sort, the masses of the constituent particles lie along well-defined Regge trajectories and the density of states within the ensemble grows exponentially as a function of the constituent-particle mass. This exponential growth is ultimately compensated by a

Boltzmann suppression factor in the primordial abundances of the individual constituents, resulting in a finite total energy density $\Omega_{tot}(t)$. We also showed that such ensembles can naturally exhibit a balancing between lifetimes and cosmological abundances of the sort required by the DDM framework.

For each such ensemble, we calculated the corresponding effective equation-of-state parameter $w_{eff}(t)$ as well as the tower fraction $\eta(t)$. We also imposed a number of zeroth-order model-independent phenomenological constraints which follow directly from knowledge of $\Omega_{tot}(t)$, $w_{eff}(t)$, and $\eta(t)$. In general, we found that the imposition of such constraints tends to introduce *correlations* between the different underlying variables which parametrize our DDM ensembles, so that an increase in one variable (such as, e.g., the exponential rate of growth in the state degeneracies) requires a corresponding shift in another variable (in this case, an increase in the lifetime of the lightest state in the ensemble, as indicated in the right panel of Fig. 5). Perhaps one of our most important results is the existence of an inverse correlation between the tower fraction $\eta(t)$ associated with a given a DDM ensemble and its corresponding fundamental mass scales, so that the present-day cosmological abundance of the dark sector must be distributed across an increasing number of different states in the ensemble as these fundamental mass scales are dialed from the Planck scale down to the GeV scale.

We are certainly not the first to consider dark-matter scenarios in which the dark matter is composite. Indeed, within the context of traditional dark-matter models, it has been appreciated for some time that the dark-matter particle could be a composite state. For example, the lightest technibaryon in technicolor theories was long ago identified as a promising dark-matter candidate [43,44], and mechanisms [45] were advanced by which this particle could be rendered sufficiently light so as to be

phenomenologically viable. Indeed, several explicit models [46] have been developed along these lines. Other more exotic baryon-like composites have also been advanced as potential dark-matter candidates [47]. Lattice studies of baryon-like states in the confining phases of both $SU(3)$ and $SU(4)$ gauge theories have also been performed [48–50].

A variety of scenarios in which a long-lived meson-like state which appears in the confining phase of a strongly-coupled hidden sector have been developed as well (for a review see, e.g., Ref. [51]). These include scenarios in which the dark-matter particle is a pseudo-Nambu-Goldstone boson (PNGB) stabilized by a dark-sector analogue of flavor symmetry [52–56] or G-parity [57], or alternatively by some other symmetry of the theory with no SM analogue [58–62]. Complementary lattice studies of strongly-coupled dark-sector scenarios in which the dark-matter candidate is a PNGB have been performed as well [63,64]. Scenarios in which the dark-matter candidate is not a PNGB, but rather a bound state of one heavy quark and one light quark, have also received recent attention [65–67], primarily due to the nonstandard direct-detection phenomenology to which they give rise, as have scenarios in which the dark-matter candidate is a bound state of heavy quarks alone [68]. More general studies of composite hidden-sector theories which give rise to meson-like or baryon-like dark-matter candidates within different regions of parameter space have also been performed [69–73].

Composite hidden-sector states consisting of non-Abelian gauge fields alone (so-called "glueball" states) have also long been recognized as promising dark-matter candidates [74,75]—a possibility which has received renewed attention [76,77] as well. Indeed, hidden sectors involving cosmologically stable dark glueball states arise naturally in a variety string constructions [78,79], as well as in certain anomaly-mediated supersymmetry-breaking scenarios [80].

In addition, the possibility that composite states in the dark sector could themselves form bound states (so-called "dark nuclei") has also been studied [81–84], as has the possibility that these nuclei themselves could combine to form dark "atoms" or even dark "molecules" [85,86]. Indeed, lattice studies [81,87] corroborate the existence of stable dark nuclei states even within simple, two-flavor models with $SU(2)$ as the confining gauge group. In such models, a dark-sector equivalent of BBN serves as the mechanism for abundance generation. Such models can have interesting phenomenological consequences, especially in the regime in which a significant fraction of the dark-matter abundance is contributed by nuclei with large nucleon numbers [88,89].

Composite dark-matter models are interesting from a phenomenological perspective as well. For example, the states of a strongly-coupled hidden sector provide a natural context [90] for strongly-interacting massive particle

(SIMP) dark matter [91,92] models, in which $3 \rightarrow 2$ processes rather than $2 \rightarrow 2$ processes play a dominant role in determining the dark-matter abundance. Indeed, a number of explicit models along these lines have been constructed [93–96]. One of the most interesting ramifications of SIMP models is that they naturally give rise to dark-matter self-interactions with cross sections sufficiently large that dark-matter scattering can have an observable impact on structure formation [97]. Such composite dark-matter models can have other phenomenological consequences as well, both at indirect-detection experiments [98,99] and at colliders [100–103]. Finally, the presence of additional non-Abelian gauge sectors, each with their own analogue of the QCD Θ-angle, could have potential implications for the physics of axions and axion-like particles [104].

While all of these represent theoretically viable possibilities for the dark sector, the dark ensemble we have considered in this paper is unique for several important reasons. In traditional composite dark-matter models, it is usually a single bound state (usually the lightest bound state) which serves as the primary dark-matter candidate and which therefore carries the full dark-matter abundance Ω_{CDM}. While there may be several other dark states to which this bound state couples—and which may play a role in determining the abundance of the dark-matter candidate—it is nevertheless true that only one (or a few) composite states carry the dark-matter abundance Ω_{CDM} and thereby play a significant role in dark-sector phenomenology. By contrast, within the DDM framework, the dark-matter abundance is potentially spread across a relatively large set of composite states with various masses and lifetimes. Thus the usual required stability of the traditional dark-matter candidate is not a required feature of the DDM ensemble, thereby allowing the associated dark-matter abundance $\Omega_{CDM}(t)$ and dark-matter equation-of-state parameter $w_{eff}(t)$ to vary with time—even during the current, matter-dominated era.

Moreover, because the DDM framework requires an enlarged viewpoint in which the entire spectrum of composite states are potentially relevant for determining the properties of the dark sector, features that describe the entire composite spectrum suddenly become relevant for determining dark-sector phenomenology—features which would not have been relevant for previous studies within more traditional frameworks. These features include the fact that the masses of such bound states actually lie along Regge trajectories, and that the densities of such bound states experience a Hagedorn-like exponential growth as a function of mass. Indeed, these features do not play a role within traditional studies of composite dark states, but they have been the cornerstones of the analysis we have presented here. In this context, we note that a similar approach was also adopted in Ref. [88] with regard to ensembles of dark nuclei whose abundances are generated

via a dark-sector analogue of BBN. This is indeed another context in which the full ensemble of dark-sector states plays an important role in dark-matter phenomenology.

Given the initial steps presented here, there are many avenues for future research. For example, in this paper we have primarily focused on the phenomenology associated with the "sweet-spot" region in Eq. (5.3), as this region gives rise to a rich spectrum of associated mass scales and DDM-like behaviors. However, other regions may also be relevant for different situations, including the case of dark ensembles emerging from the bulk sectors of actual critical Type I string theories. Indeed, such theories typically have significantly larger central charges and values of $D_\perp$ than those corresponding to the $D_\perp = 2$ flux tube, and thus correspond to values of (B, C) which are very far from the "benchmark" values in Eq. (5.2). Such strings also likely correspond to values of (r, s) which are far from those in Eq. (5.3). Likewise, in our analysis we have taken $\kappa = 1$ and $\xi = 3$. Although these simple choices were well-motivated and conservative, it would certainly be interesting to explore the consequences of alternative choices. It would also be of interest to explore the ramifications of relaxing some of the approximations we have made in our analysis. These include the "instantaneous freeze-out" approximation that underpins the Boltzmann suppression factor in Eq. (3.1), as well as our implicit assumption that the Hubble expansion within which our calculations have taken place is unaffected by potential gravitational back-reaction from our continually evolving dark sector. While these approximations may certainly be justified to first order, a more refined calculation is still capable of altering our results numerically if not qualitatively.

It would also be interesting to subject the DDM ensembles we have studied here to more detailed phenomenological constraints. The constraints we have studied here, such as our look-back and w_{eff} constraints, are those that follow directly (and in a completely model-independent manner) from knowledge of $\Omega_{tot}(t)$ and $w_{eff}(t)$ alone, and as such we have seen that they are sufficient to rule out vast regions of parameter space. It is nevertheless true that a plethora of additional constraints could be formulated once a particular scenario with a particular particle content is specified, and that imposing such additional constraints could potentially narrow our viable parameter space still further.

Finally, and perhaps most importantly, in this paper we have assumed that the effects of *intra-ensemble* decays on the decay widths of the ensemble constituents are negligible. Such an assumption is certainly consistent with our other assumptions about the structure of the theory. In general, following our string-based approach to understanding the dyamics of these bound-state flux tubes, we may regard the strength of the interactions among the different dark hadrons in our DDM model as being governed by an additional parameter, a so-called "string coupling" g_s, which we have not yet specified but which does not impact any of the results we have presented thus far. In general, g_s can be different from the coupling which governs the decays of our ensemble states to SM states and which is thus embedded within τ_0. In an actual string construction, the value of g_s is determined by the vacuum expectation value (VEV) of the dilaton field, but the dynamics that determines this VEV is not well understood. In general, however, intra-ensemble decays will provide an additional contribution to the total decay widths Γ_n, especially for the heavier ensemble constituents, and the decays of these heavier constituents can serve as an additional source for the abundances of the lighter constituents. The effects of such intra-ensemble decays will be discussed in more detail in Ref. [105].

[1] K. R. Dienes and B. Thomas, Phys. Rev. D **85**, 083523 (2012).

[2] K. R. Dienes and B. Thomas, Phys. Rev. D **85**, 083524 (2012).

[3] K. R. Dienes, S. Su, and B. Thomas, Phys. Rev. D **86**, 054008 (2012).

[4] K. R. Dienes, S. Su, and B. Thomas, Phys. Rev. D **91**, 054002 (2015).

[5] K. R. Dienes, J. Kumar, and B. Thomas, Phys. Rev. D **86**, 055016 (2012).

[6] K. R. Dienes, J. Kumar, and B. Thomas, Phys. Rev. D **88**, 103509 (2013).

[7] K. K. Boddy, K. R. Dienes, D. Kim, J. Kumar, J. C. Park, and B. Thomas, Phys. Rev. D **94**, 095027 (2016).

[8] K. K. Boddy, K. R. Dienes, D. Kim, J. Kumar, J. C. Park, and B. Thomas, arXiv:1609.09104.

[9] K. R. Dienes and B. Thomas, Phys. Rev. D 86, 055013 (2012).

[10] K. R. Dienes, J. Fennick, J. Kumar, and B. Thomas (work in progress).

[11] K. R. Dienes, J. Fennick, J. Kumar, and B. Thomas, Phys. Rev. D 93, 083506 (2016).

[12] R. Hagedorn, Nuovo Cimento Suppl. 3, 147 (1965).

[13] For reviews, see, e.g., M. B. Green, J. A. Schwarz, and E. Witten, *Superstring Theory*, Vols. I and II (Cambridge University Press, Cambridge, England, 1987); J. Polchinski, *String Theory*, Vols. I and II (Cambridge University Press, Cambridge, England, 1998).

[14] K. R. Dienes and J. R. Cudell, Phys. Rev. Lett. 72, 187 (1994).

[15] G. H. Hardy and S. Ramanujan, Proc. London Math. Soc. s2-17, 75 (1918).

[16] I. Kani and C. Vafa, Commun. Math. Phys. 130, 529 (1990).

[17] K. R. Dienes, Nucl. Phys. B429, 533 (1994).

[18] Y. Nambu (unpublished, 1970).

[19] P. Ramond, Phys. Rev. D 3, 2415 (1971).

[20] A. Neveu and J. H. Schwarz, Nucl. Phys. B31, 86 (1971).

[21] A. M. Polyakov, Nucl. Phys. B268, 406 (1986).

[22] M. B. Green, Phys. Lett. B 266, 325 (1991).

[23] J. Polchinski and A. Strominger, Phys. Rev. Lett. 67, 1681 (1991).

[24] P. A. R. Ade *et al.* (Planck Collaboration), Astron. Astrophys. 594, A13 (2016).

[25] L. Anderson *et al.* (BOSS Collaboration), Mon. Not. R. Astron. Soc. 441, 24 (2014).

[26] N. Suzuki, D. Rubin, C. Lidman, G. Aldering, R. Amanullah, K. Barbary, L. F. Barrientos, J. Botyanszki *et al.*, Astrophys. J. 746, 85 (2012).

[27] R. H. Cyburt, J. Ellis, B. D. Fields, F. Luo, K. A. Olive, and V. C. Spanos, J. Cosmol. Astropart. Phys. 10 (2009) 021.

[28] W. Hu and J. Silk, Phys. Rev. D 48, 485 (1993).

[29] W. Hu and J. Silk, Phys. Rev. Lett. 70, 2661 (1993).

[30] T. R. Slatyer, Phys. Rev. D 87, 123513 (2013).

[31] L. Accardo *et al.* (AMS Collaboration), Phys. Rev. Lett. 113, 121101 (2014).

[32] AMS-02 Collaboration, presentations at AMS Days at CERN, 2015 (unpublished).

[33] A. H. G. Peter, C. E. Moody, and M. Kamionkowski, Phys. Rev. D 81, 103501 (2010).

[34] M. Y. Wang, A. H. G. Peter, L. E. Strigari, A. R. Zentner, B. Arant, S. Garrison-Kimmel, and M. Rocha, Mon. Not. R. Astron. Soc. 445, 614 (2014).

[35] M. Y. Wang and A. R. Zentner, Phys. Rev. D 82, 123507 (2010).

[36] Y. Gong and X. Chen, Phys. Rev. D 77, 103511 (2008).

[37] G. Blackadder and S. M. Koushiappas, Phys. Rev. D 90, 103527 (2014).

[38] S. De Lope Amigo, W. M. Y. Cheung, Z. Huang, and S. P. Ng, J. Cosmol. Astropart. Phys. 06 (2009) 005.

[39] B. Audren, J. Lesgourgues, G. Mangano, P. D. Serpico, and T. Tram, J. Cosmol. Astropart. Phys. 12 (2014) 028.

[40] E. Aubourg *et al.*, Phys. Rev. D 92, 123516 (2015).

[41] G. Blackadder and S. M. Koushiappas, Phys. Rev. D 93, 023510 (2016).

[42] V. Poulin, P. D. Serpico, and J. Lesgourgues, J. Cosmol. Astropart. Phys. 08 (2016) 036.

[43] S. Nussinov, Phys. Lett. 165B, 55 (1985).

[44] S. M. Barr, R. S. Chivukula, and E. Farhi, Phys. Lett. B 241, 387 (1990).

[45] S. B. Gudnason, C. Kouvaris, and F. Sannino, Phys. Rev. D 73, 115003 (2006).

[46] T. A. Ryttov and F. Sannino, Phys. Rev. D 78, 115010 (2008).

[47] K. Harigaya, T. Lin, and H. K. Lou, J. High Energy Phys. 09 (2016) 014.

[48] T. Appelquist *et al.* (Lattice Strong Dynamics (LSD) Collaboration), Phys. Rev. D 89, 094508 (2014).

[49] T. Appelquist *et al.*, Phys. Rev. D 92, 075030 (2015).

[50] T. Appelquist *et al.*, Phys. Rev. Lett. 115, 171803 (2015).

[51] G. D. Kribs and E. T. Neil, Int. J. Mod. Phys. A 31, 1643004 (2016).

[52] C. Kilic, T. Okui, and R. Sundrum, J. High Energy Phys. 02 (2010) 018.

[53] T. Hur and P. Ko, Phys. Rev. Lett. 106, 141802 (2011).

[54] M. Holthausen, J. Kubo, K. S. Lim, and M. Lindner, J. High Energy Phys. 12 (2013) 076.

[55] H. Hatanaka, D. W. Jung, and P. Ko, J. High Energy Phys. 08 (2016) 094.

[56] Y. Ametani, M. Aoki, H. Goto, and J. Kubo, Phys. Rev. D 91, 115007 (2015).

[57] Y. Bai and R. J. Hill, Phys. Rev. D 82, 111701 (2010).

[58] M. R. Buckley and E. T. Neil, Phys. Rev. D 87, 043510 (2013).

[59] M. Heikinheimo, A. Racioppi, M. Raidal, C. Spethmann, and K. Tuominen, Mod. Phys. Lett. A 29, 1450077 (2014).

[60] S. Bhattacharya, B. Melić, and J. Wudka, J. High Energy Phys. 02 (2014) 115.

[61] A. Carmona and M. Chala, J. High Energy Phys. 06 (2015) 105.

[62] M. Frigerio, A. Pomarol, F. Riva, and A. Urbano, J. High Energy Phys. 07 (2012) 015.

[63] R. Lewis, C. Pica, and F. Sannino, Phys. Rev. D 85, 014504 (2012).

[64] A. Hietanen, C. Pica, F. Sannino, and U. I. Sondergaard, Phys. Rev. D 87, 034508 (2013).

[65] D. S. M. Alves, S. R. Behbahani, P. Schuster, and J. G. Wacker, Phys. Lett. B 692, 323 (2010).

[66] M. Lisanti and J. G. Wacker, Phys. Rev. D 82, 055023 (2010).

[67] D. Spier Moreira Alves, S. R. Behbahani, P. Schuster, and J. G. Wacker, J. High Energy Phys. 06 (2010) 113.

[68] G. D. Kribs, T. S. Roy, J. Terning, and K. M. Zurek, Phys. Rev. D 81, 095001 (2010).

[69] O. Antipin, M. Redi, and A. Strumia, J. High Energy Phys. 01 (2015) 157.

[70] O. Antipin, M. Redi, A. Strumia, and E. Vigiani, J. High Energy Phys. 07 (2015) 039.

[71] Y. Bai and P.~Schwaller, Phys. Rev. D 89, 063522 (2014).

[72] P. Schwaller, D. Stolarski, and A. Weiler, J. High Energy Phys. 05 (2015) 059.

[73] P. Schwaller, Phys. Rev. Lett. 115, 181101 (2015).

[74] L. B. Okun, Pis'ma Zh. Eksp. Teor. Fiz. 31, 156 (1979) [JETP Lett. 31, 144 (1980)].

[75] L. B. Okun, Nucl. Phys. B173, 1 (1980).

[76] A. Soni and Y. Zhang, Phys. Rev. D 93, 115025 (2016).

[77] L. Forestell, D. E. Morrissey, and K. Sigurdson, arXiv:1605.08048.
[78] A. E. Faraggi and M. Pospelov, Astropart. Phys. **16**, 451 (2002).
[79] J. Halverson, B. D. Nelson, and F. Ruehle, arXiv:1609.02151.
[80] J. L. Feng and Y. Shadmi, Phys. Rev. D **83**, 095011 (2011).
[81] W. Detmold, M. McCullough, and A. Pochinsky, Phys. Rev. D **90**, 115013 (2014).
[82] G. Krnjaic and K. Sigurdson, Phys. Lett. B **751**, 464 (2015).
[83] R. Foot and S. Vagnozzi, Phys. Rev. D **91**, 023512 (2015).
[84] R. Foot and S. Vagnozzi, J. Cosmol. Astropart. Phys. 07 (2016) 013.
[85] J. M. Cline, Z. Liu, G. Moore, and W. Xue, Phys. Rev. D **90**, 015023 (2014).
[86] K. K. Boddy, M. Kaplinghat, A. Kwa, and A. H. G. Peter, Phys. Rev. D **94**, 123017 (2016).
[87] W. Detmold, M. McCullough, and A. Pochinsky, Phys. Rev. D **90**, 114506 (2014).
[88] E. Hardy, R. Lasenby, J. March-Russell, and S. M. West, J. High Energy Phys. 06 (2015) 011.
[89] E. Hardy, R. Lasenby, J. March-Russell, and S. M. West, J. High Energy Phys. 07 (2015) 133.
[90] Y. Hochberg, E. Kuflik, T. Volansky, and J. G. Wacker, Phys. Rev. Lett. **113**, 171301 (2014).
[91] E. D. Carlson, M. E. Machacek, and L. J. Hall, Astrophys. J. **398**, 43 (1992).
[92] A. A. de Laix, R. J. Scherrer, and R. K. Schaefer, Astrophys. J. **452**, 495 (1995).
[93] Y. Hochberg, E. Kuflik, H. Murayama, T. Volansky, and J. G. Wacker, Phys. Rev. Lett. **115**, 021301 (2015).
[94] M. Hansen, K. Langæble, and F. Sannino, Phys. Rev. D **92**, 075036 (2015).
[95] N. Bernal and X. Chu, J. Cosmol. Astropart. Phys. 01 (2016) 006.
[96] A. Kamada, M. Yamada, T. T. Yanagida, and K. Yonekura, Phys. Rev. D **94**, 055035 (2016).
[97] K. K. Boddy, J. L. Feng, M. Kaplinghat, and T. M. P. Tait, Phys. Rev. D **89**, 115017 (2014).
[98] K. K. Boddy, J. L. Feng, M. Kaplinghat, Y. Shadmi, and T. M. P. Tait, Phys. Rev. D **90**, 095016 (2014).
[99] M. Freytsis, D. J. Robinson, and Y. Tsai, Phys. Rev. D **91**, 035028 (2015).
[100] H. M. Lee and M. S. Seo, Phys. Lett. B **748**, 316 (2015).
[101] Y. Hochberg, E. Kuflik, and H. Murayama, J. High Energy Phys. 05 (2016) 090.
[102] C. Englert, K. Nordstrom, and M. Spannowsky, Phys. Rev. D **94**, 055028 (2016).
[103] S. Bruggisser, F. Riva, and A. Urbano, arXiv:1607.02474.
[104] P. Di Vecchia and F. Sannino, Eur. Phys. J. Plus **129**, 262 (2014).
[105] K. R. Dienes, F. Huang, J. Kost, S. Su, and B. Thomas (work in progress).